Human sensory neurons exhibit cell-type-specific, pain-associated differences in intrinsic excitability and expression of *SCN9A* and *SCN10A*

Author list

Jiwon Yi[1, 2], Lite Yang[1,2], Allie J. Widman[1], Alexa Toliver[1], Zachariah Bertels[1], John Smith Del Rosario[1], Richard A. Slivicki[1], Maria Payne[1], Adam J. Dourson[1], Jun-Nan Li[1], Rakesh Kumar[1], Prashant Gupta[1], Juliet M. Mwirigi[1], Alexander Chamessian[1], John Lemen[3], Bryan A. Copits[1], Robert W. Gereau IV[1,4]*

[1] Department of Anesthesiology, Washington University Pain Center, Washington University School of Medicine, St. Louis, MO, United States

[2] Neuroscience Graduate Program, Division of Biology & Biomedical Sciences, Washington University School of Medicine, St. Louis, MO, United States

[3] Mid-America Transplant, St. Louis, MO, United States

[4] Department of Neuroscience, Washington University, St. Louis, MO, United States

*Corresponding author. Address: Department of Anesthesiology, Washington University Pain Center, Washington University School of Medicine, 660 South Euclid Avenue Campus Box 8054, St. Louis, 63110, MO, United States. E-mail: gereaur@wustl.edu (R.W. Gereau). Phone: (314) 362-8312. URL: pain.wustl.edu

Conflict of interest statement: The authors have declared that no conflict of interest exists.

Abstract

Despite the prevalence of chronic pain, the approval of novel, non-opioid therapeutics has been slow. A major translational challenge in analgesic development is the difference in gene expression and functional properties between human and rodent dorsal root ganglia (DRG) sensory neurons. Extensive work in rodents suggests that sensitization of nociceptors in the DRG is essential for the pathogenesis and persistence of pain; however, direct evidence demonstrating similar physiological sensitization in humans is limited. Here, we examine whether pain history is associated with nociceptor hyperexcitability in human DRG (hDRG). We identified three electrophysiologically distinct clusters (E-types) of hDRG neurons based on firing properties and membrane excitability. Combining electrophysiological recordings and single-cell RNA-sequencing ("Patch-seq"), we linked these E-types to specific transcriptionally defined nociceptor subpopulations. Comparing hDRG neurons from donors with and without evident pain history revealed cluster-specific, pain history-associated differences in hDRG excitability. Finally, we found that hDRG from donors with pain history express higher levels of transcripts encoding voltage-gated sodium channel 1.7 (NaV1.7) and 1.8 (NaV1.8) which specifically regulate nociceptor excitability. These findings suggest that donors with pain history exhibit distinct hDRG electrophysiological profiles compared to those without pain history and further validate NaV1.7 and 1.8 as targets for analgesic development.

Introduction

Chronic pain affects an estimated 20% of people worldwide and is a major cause of disability(1–4). While much effort has been placed on developing efficacious and non-addictive analgesics, available options for non-opioid pharmacotherapy are still limited(5). Recent studies have identified major differences in nociceptor neurobiology between rodents and humans(6–16), which may contribute to the translational challenges of analgesic development. This illustrates a critical need to better understand the physiology of human sensory neurons.

The dorsal root ganglion (DRG) comprises multiple functionally specialized populations of sensory neurons, including nociceptors that detect noxious stimuli(17). In rodent DRG, at least 2-3 physiologically distinct clusters of nociceptors with different spike firing patterns (e.g., single vs. repetitive), action potential waveforms, and other membrane properties have been identified(17, 18). There is increasing evidence that similar clusters of single- and repetitively-firing neurons exist in the human DRG (19, 20). However, little is known about how these physiological clusters of hDRG map onto functionally and transcriptionally defined subpopulations.

Nociceptor hyperactivity following injury or inflammation is thought to be a critical component in the development and/or maintenance of pain (21, 22). Ectopic spontaneous activity and hyperexcitability have been reported in preclinical animal models of both neuropathic and inflammatory pain (18, 23–27). Additionally, there is emerging evidence that human sensory neurons from patients with neuropathic pain and erythromelalgia also exhibit persistent hyperactivity (27–31); however, whether similar hyperexcitability of the hDRG is seen in other pain conditions with different pathobiology, such as musculoskeletal pain, is yet unknown.

Recent evidence also suggests that the presence of pain-associated hyperactivity in nociceptors is variable among different functional cell classes. For instance, nerve injury only induces sensitization and spontaneous activity in non-accommodating (repetitively firing) subpopulation of nociceptors, but not in the rapidly accommodating (single spiking) nociceptors,

in rats (18). Similarly, hDRG neurons have been shown to have differential responses to bradykinin, an inflammatory mediator implicated in pain pathogenesis, based on their spiking patterns (19). However, whether electrophysiologically distinct subpopulations of *human* nociceptors show pain-associated hyperexcitability has not been examined in depth.

In this study, we address these gaps through patch-clamp electrophysiology paired with single-cell RNA sequencing (Patch-seq), in addition to *in situ* hybridization from hDRG obtained from donors with and without pain history. We find that there are multiple physiologically distinct subpopulations of human sensory neurons, and that these subpopulations can be broadly mapped onto different transcriptionally defined clusters. We also show that pain history is associated with bidirectional, cluster-specific differences in the intrinsic excitability of hDRG neurons. Finally, hDRG tissue from donors with pain history show enriched expression of *SCN9A* and *SCN10A*, genes that encode for NaV1.7 and NaV1.8, respectively, which likely contribute to pain-associated hyperexcitability seen in these hDRG neurons. Together, these findings suggest that hDRG neurons show physiological specialization which may be associated with both functional diversity and pain-associated differences in excitability.

Results

Physiologically distinct clusters of small- and medium-sized human sensory neurons

Previous studies have reported that rodent nociceptors display 2-3 physiological phenotypes in culture(17, 18, 32). Here, we tested whether such heterogeneity in membrane excitability and firing pattern also exists in human sensory neuron cultures. To increase the likelihood of recording from nociceptors, we recorded from hDRG neurons with diameter <60 μm based on prior work demonstrating enrichment of various nociceptor populations among small- to medium-sized human sensory neurons (11). hDRG neurons with resting membrane potential >30mV, or an unstable resting membrane potential, were considered to be unhealthy and recordings from those cells were excluded from analysis for quality control.

Using hDRG obtained postmortem from organ donors (Table 1), we identified three electrophysiological phenotypes (E-types) of human sensory neurons based on their distinct spike-firing patterns in response to depolarizing current steps (Figure 1A-C). Neurons that fired multiple action potentials in response to current injections between 50 pA – 2 nA were classified as repetitive spikers (Figure 1A, D, E); 42.9% of all recorded hDRG neurons were found to be repetitive spikers. Neurons that did not fire more than 1 action potential in response to a 2 nA current step were classified as single spikers and represented 55.4% of the hDRG neurons (Figure 1D, E). Finally, we identified two neurons that displayed anode-break excitation following hyperpolarizing current steps and rapid, burst-like firing of 1-2 spikes in response to suprathreshold current injection; we classified these as “burst” firing neurons (Figure 1C-E). hDRG neurons with the repetitive, single, and burst-firing E-types did not significantly differ in size or in the number of days they were in culture prior to recording (Table 2, Supplementary Figure 2). Due to the small number of burst-firing neurons in our dataset (n=2 neurons), subsequent comparisons of electrophysiological parameters were only conducted between the repetitive and single-spiking groups.

The repetitive and single-spiking E-types diverged in their intrinsic excitability, membrane properties, and spike kinetics. Repetitive spikers fired a larger number of action potentials at suprathreshold currents compared to single spikers (Figure 1E). Additionally, repetitive-spiking neurons displayed a significantly lower rheobase and higher input resistance than single-spiking neurons, indicative of greater membrane excitability (Figure 1F, G; Table 2). Repetitive- and single-spiking E-types also exhibited differences in action potential kinetics and waveform: single spikers had a faster action potential decay and a narrower half-width of the action potential compared to the two repetitive firing E-types (Figure 1H-J, Table 2). The two E-types did not significantly differ in resting membrane potential, voltage sag ratio, action potential threshold, spike amplitude, or slope of the rising phase (Table 2).

The repetitive spikers were further subdivided based on the presence of spike amplitude accommodation (reduction in amplitude in a train of multiple spikers, as seen in Figure 1A) and spike-frequency adaptation (decrease in firing rate in response to sustained current stimulus) at suprathreshold currents, associated with sodium channel block at high current steps (Figure 1A, Supplementary Figure 1). Repetitive spikers that showed amplitude accommodation and frequency adaptation were identified as having an inverse-U-shaped input-output curve, whereas the non-adapting subset displayed a linear input-output relationship (Supplementary Figure 1A). Additionally, the repetitive-adapting neurons displayed lower rheobase relative to repetitive-non-adapting neurons (Supplementary Figure 1C); these two observations demonstrate that the adapting subtype require lower current injections to reach threshold to start firing, and that they reach peak spike firing at much lower current injections compared to the non-adapting neurons. Other membrane properties, including input resistance, action potential threshold, and resting membrane potential, were not significantly different between the groups (Supplementary Figure 1C-G). These results suggest that the repetitive spiking neurons that have spike frequency adaptation are more excitable than the repetitive spiking neurons that do not display such

frequency adaptation.

Next, we used principal component analysis (PCA) to determine whether hDRG neurons can be clustered based on their electrophysiological properties (Figure 2). Features related to membrane excitability, such as rheobase, and those related to spike kinetics, such as maximum decay and rise slopes and amplitude, were found to have the largest contributions to PC1 and PC2 (Figure 2A). Using K-means neighbor clustering, hDRGs were separated into three clusters (Figure 2B). When the cluster assignment was compared to the E-type of each cell, we found that the cluster assignments roughly corresponded to the E-type, whereby the majority of hDRG neurons in Cluster 1 (20/21 cells, or 95.2%) and Cluster 3 (36/46 cells, or 78.3%) were single spikers, and the majority of the Cluster 2 neurons (37/43 cells, or 86.0%) were repetitive spikers. Similarly, 90.3% of single-spiking neurons were found to be in either Cluster 3 (36/62 single spikers, or 58.1%) or Cluster 1 (20/62 single spikers, or 32.2%), while 77.1% (37/48 repetitive spikers) of repetitive-firing neurons were found to be in Cluster 2. Together, these results suggest that hDRG neurons can be clustered based on their membrane properties and spike kinetics, and that those clusters broadly correlate with their firing patterns.

Patch-seq identifies four transcriptionally distinct populations of human DRG

While recent single-cell RNA sequencing (scRNA-seq) studies have revealed diverse transcriptionally defined populations of human DRG sensory neurons, it remains elusive whether distinct firing patterns are linked to specific transcriptionally defined populations (1–4). Therefore, we performed Patch-seq studies that allowed us to examine correlations between E-types and transcriptional types from the same cells (33). After patch-clamp recording, we performed RNA-seq on the cytosolic contents extracted from individual recorded cells (Figure 3A, Supplementary Figure 3A). To control the sample quality, we set up cDNA quality control (QC) cutoffs (total cDNA yield higher than 2 ng and at least 35% of the cDNA falling within the size range of 500-6000 bp) that well sperate the positive/negative controls (Supplementary Figure 3B). Samples that passed

the cDNA QC showed significantly better sequencing metrices and overall stronger transcriptional correspondence to their firing properties, compared to those that failed QC and negative controls (Supplementary Figure 3C, D). We identified a total of 69 Patch-seq samples that passed cDNA QC metrics and included them in the transcriptional analysis.

Despite the recent efforts for elucidating the transcriptional profiles of individual human DRG neuronal types, the evidence to provide the ground truth about their cytosolic RNA diversity is lacking, hampering our understanding of the transcriptional profile of the Patch-seq samples. To aid the Patch-seq gene expression data analysis, we compared the average expression of all detected genes across Patch-seq samples to the average expression of those genes across neurons and non-neuronal cells from several published scRNA-seq datasets with varying starting materials for sequencing (e.g. single-nucleus, single-cell, and single-soma) (Supplementary Figure 3E) (11, 14, 34–36). The Patch-seq gene expression best correlated with the single-soma RNA-seq data among all datasets examined (35). Therefore, we used the cell types and their marker genes identified in the single-soma RNA-seq dataset (35) to guide our transcriptional analysis.

To study the transcriptional cell types of human DRG, we performed clustering analysis on the Patch-seq gene expression data, which revealed four transcriptionally distinct clusters (Figure 3B). Using the marker genes previously reported (Supplementary Figure 4)(34, 37), we mapped each cluster to major human DRG cell classes (Figure 3C). **Cluster one** exhibited low expression level of *CALCA* (calcitonin related polypeptide alpha), encoding Calcitonin Gene-Related Peptide (CGRP), and high expression levels of *NTRK3* (neurotrophic receptor tyrosine kinase 3) and *FXYD7* (FXYD domain containing ion transport regulator 7), thus transcriptionally corresponding to A-LTMRs (A-fiber low-threshold mechanoreceptors). **Cluster two** expresses *CALCA*, *FXYD7,* and *NTRK1* (neurotrophic receptor tyrosine kinase 1) and corresponds to A-PEP (peptidergic A-fiber). **Cluster three** highly expresses *CALCA*, *NTRK1*, and *INA* (internexin

neuronal intermediate filament protein alpha), indicating that their overall transcriptional profiles are most similar to C-PEP (peptidergic C-fiber). Notably, a subset of samples in cluster three highly express the C-NP (non-peptidergic C-fiber) marker *FXYD6* with no or extremely low expression of *CALCA* (Figure 3C, Supplementary Figure 4D, E), suggesting that cluster three likely contains a mixture of C-PEP and C-NP neurons. **Cluster four** lacks the expression of neuronal marker genes while uniquely expressing non-neuronal marker genes, such as *APOE* (apolipoprotein E) (Figure 3C, D). Therefore, cluster four represents samples of non-neuronal transcriptional profiles. Three samples in cluster four are likely non-neuronal cells as they did not elicit action potentials during Patch-clamp recording (Figure 3F), whereas the remaining samples are likely neurons with glial contamination during the cytosol extraction process. To further validate the cell type annotation of the Patch-seq samples, we performed integration analysis of samples assigned to neuronal clusters (clusters 1-3) with single-soma RNA-seq data (Figure 3E). Patch-seq samples from each cluster are well mapped to the four DRG neuron classes described previously. Taken together, we differentiate our Patch-seq samples into three major neuron classes: A-LTMRs (cluster one), A-PEP (cluster two), and C-fiber neurons (cluster three) based on their gene expression.

Patch-seq maps repetitive- and single-spiking hDRG neurons to distinct transcriptionally defined populations

The DRG sensory neurons are composed of multiple subpopulations that vary in gene expression, modality-specificity, and conduction velocity(11, 36, 38–42). We next asked whether single- and repetitive-spiking nociceptors in our dataset belonged to transcriptionally distinct subpopulations. There are in total 54 Patch-seq samples that passed both electrophysiology and sequencing QC and thus were assigned both E-type and transcriptional clusters. Among them, single- and repetitive-firing neurons make up 66.7% (36 neurons) and 28.6% (15 neurons) of the total population, respectively, and are present in all transcriptional clusters (Figure 3F). In transcriptional clusters one and two, which correspond to A-LTMR and A-PEP, respectively,

single-firing neurons constitute 76.9% and 80% of the population in each cluster and are over-represented by 1.47-fold and 1.53-fold (hypergeometric p-values = 0.05 and 0.01), respectively. Conversely, repetitive-spiking neurons make up 43.8% of the population and are over-represented by 2.01-fold (hypergeometric p-value = 0.02) in transcriptional cluster three (C-NP and C-PEP). These results suggest that A-fiber DRG neurons have a high proportion of single-spiking neurons and C-fiber neurons are enriched in repetitive-spiking neurons.

To better understand the molecular markers and functions of single- and repetitive-spiking neurons, we performed differential expression analysis between the Patch-seq samples of the two E-types and identified their enriched gene ontology terms (Figure 3G, I). Notably, *TAC1* (Tachykinin Precursor 1) and *TRPA1* (Transient Receptor Potential Cation Channel Subfamily A Member 1) were found to be more highly expressed in repetitive-spiking neurons than single-spiking neurons (Figure 3H). *TAC1* encodes substance P, which has been shown to involved in chronic pain. *TAC1* expression is 3.5-folder higher in repetitive-spiking neurons compared to single-spiking neurons (FDR = 2.4E-05); *TRPA1* encodes the noxious cold-activated channel, *TRPA1* is 4-fold higher in repetitive-spiking neurons compared to single-spiking neurons (FDR = 0.01) (43, 44). Interesting, in available scRNA-seq data of human sensory neurons, *TAC1* and *TRPA1* are highly expressed in C-PEP cell types, suggesting that repetitive-spiking neurons may be enriched for C-PEP neurons (34, 35). While each Patch-seq transcriptional cluster and cell class identified in this study may correspond to multiple transcriptionally and functionally distinct DRG cell types, future studies will be required to map E-types to individual sensory neuronal cell types.

Donor pain history is associated with changes in membrane excitability in repetitive- and single-spiking clusters of human sensory neurons.

In rodents, pain-inducing injuries have been shown to cause hyperexcitability in nociceptors in a physiological cluster (E-type)-specific manner (18). While pain-associated

hyperexcitability and ectopic activity in hDRG has been similarly reported in samples resected from cancer patients (28–30), it is unknown whether there are E-type-specific differences in intrinsic excitability associated with pain history in the nociceptor population, or whether pain-associated hyperexcitability can also be detected in samples from individuals with diverse pain etiologies. Therefore, we tested whether a donor's history of pain, as reported by their next-of-kin (Table 1), was associated with any differences in membrane excitability and kinetics of repetitive and single-firing clusters of small- to medium-diameter hDRG neurons.

Donors were classified as having no significant pain history ("No Pain Hx") or having a significant pain history in the dermatome of thoracolumbar DRGs ("Pain Hx") based on their medical history (Table 1). A donor was classified as having significant pain history if they met two out of three of the following criteria: (a) the word "pain" is used to describe donor's recent or present medical condition (e.g., "daily pain," "regular pain," "painful tendonitis,"), and the dermatome of pain is specified to be in the back and/or the lower body; (b) donor's medical history includes prescribed use of analgesics (e.g., hydrocodone or gabapentin) that is unrelated to substance use disorder, or there is documentation of other non-pharmaceutical interventions for pain (e.g., back surgery, nerve blocks); (c) donor's medical history includes a disorder for which pain is a major symptom, such as arthritis or scleroderma. Based on these inclusion criteria, eight donors were identified as having a significant pain history ("Pain Hx"). Musculoskeletal pain was the predominant cause for complaint in the Pain Hx donors (77.8%, or 7/9 donors; Table 1). While the average age of the Pain Hx donors trended higher (48.8 ± 4.7 years) compared to the No Pain Hx group (38.2 ± 3.4 years, this difference was not significant ($p = 0.083$, one-way ANOVA). Both groups had similar proportions of repetitive and single-spikers (Table 3), suggesting that the overall distribution of repetitive and single-spiking clusters does not vary across the three groups.

Pain history was associated cluster-specific differences in the intrinsic excitability and kinetics of hDRG neurons (Figure 4). In repetitive spikers, neurons from Pain Hx group showed

an upward and leftward shift in the input-output curve in comparison with neurons from the No Pain Hx group (Figure 4A). This indicates that neurons from the Pain Hx group fired more action potentials in response to current steps compared to neurons from the No Pain Hx group (Figure 4A). Pain history was also associated with a more hyperpolarized action potential threshold and a lower rheobase compared to the No Pain Hx group (Figure 4B, C), which are indicative of hyperexcitability. Surprisingly, neurons from donors with Pain Hx exhibited a more hyperpolarized resting membrane potential compared to neurons from donors with No Pain Hx (Figure 4D). Within the repetitive spiking neurons, hDRG neurons from donors with Pain Hx had a higher percentage of neurons that demonstrated spike frequency adaptation (71.4% adapting neurons in Pain Hx vs. 39.3% adapting neurons in No Pain Hx; Figure 4E), a feature associated with higher spike firing rate at lower current injections compared to repetitive spikers that do not show spike frequency adaptation (Supplementary Figure 1). There were no significant differences in the action potential kinetics of repetitive spikers from the three groups (Table 4).

In single spikers, pain history was associated with a rightward shift in the input-output curve, indicative of lower action potential firing (Figure 4F). There was no significant difference in the rheobase between the Pain Hx and No Pain Hx groups (Figure 4G). Single spikers from Pain Hx group additionally had a more depolarized resting membrane potential, narrower half-width, and faster rise and decay phases (Figure 4H-K; Table 4). These differences point to a narrowing of the action potential waveform in single spikers from the Pain Hx group compared to the No Pain Hx group.

Together, these results demonstrate that human sensory neurons from donors with Pain Hx show differences in the intrinsic excitability and spike kinetics compared to sensory neurons from donors without major history of pain, where the excitability of the more excitable, repetitive-spiking cluster is enhanced, while the less excitable, single-spiking cluster shows reduced excitability.

Pain history is associated with higher NaV1.7 and 1.8 expression in human sensory neurons

Given the differences in the membrane excitability and kinetics we observed in the hDRG neurons from pain donors, we investigated whether there were any differences in the expression of voltage-gated sodium channels NaV1.7, 1.8, and 1.9. These three channels are selectively expressed in the peripheral nervous system, act as key modulators of nociceptor excitability, and are thought to drive neuronal hypersensitivity that underlies persistent pain (45). Analysis of previously published DRG whole-tissue bulk transcriptomics data (30) revealed no significant difference in the expression of the genes *SCN9A* (encodes NaV1.7), *SCN10A* (encodes NaV1.8), and *SCN11A* (encodes NaV1.9), between cancer patients with pain and cancer patients without pain (Supplementary Figure 5). However, as whole-tissue sequencing can dilute changes that occur at the single-cell level, we utilized RNAScope *in situ* hybridization to examine *SCN9A, SCN10A,* and *SCN11A* expression in our donor population. *SCN9A, SCN10A,* and *SCN11A* expression level in the DRG was quantified in two ways: (1) the overall percentage of DRG neurons that express the target gene, and (2) the relative expression level (e.g., number of mRNA copies of target gene) within each target gene-expressing neuron.

We found that the Pain Hx group tended to have a higher proportion of neurons expressing *SCN9A* and *SCN10A* compared to the No Pain Hx group, though the difference was not statistically significant (Figure 5A-B, E-F). The average number of mRNA copies detected in each hDRG neuron was higher in the Pain Hx group compared to the No Pain Hx group (Figure 5C, G). The increased within-cell expression of *SCN9A* and *SCN10A* was seen across multiple different sizes of cells (Figure 5D, H). *SCN11A* expression tended towards higher expression in the Pain Hx group compared to the No Pain Hx group as measured in terms of proportion and within-cell expression (Figure 5I-K) but without statistical significance. Interestingly, *SCN9A*, but not *SCN10A* or *SCN11A*, was detected in satellite glial cells surrounding neuronal cell bodies (Supplementary Figure 6), confirming previous observations(29, 37).

Discussion

In the present study, we provide a detailed electrophysiological characterization of human DRG neurons. Using Patch-seq, we demonstrate that electrophysiologically-defined clusters can be linked to transcriptionally defined subpopulations of hDRG neurons, and that a majority of small-to-medium neurons patched in our study belong to the nociceptor population. Additionally, we show that pain history is associated with differences in sensory neuron physiology that is dependent on the electrophysiological phenotype, with repetitive spikers from Pain Hx donors demonstrating hyperexcitability compared to repetitive spikers from No Pain Hx donors. Finally, we show that there is greater expression of Nav1.7 and NaV1.8 in lumbar DRGs from donors with documented pain history, which may contribute to pain-associated hyperexcitability. In the context of previous studies (18, 23–30) our findings suggest that pain-associated dysregulation of nociceptor excitability is seen in both humans and rodents, and across different pain pathologies.

Physiological heterogeneity of sensory neurons from donors without history of pain

Similar to prior reports in rodents(17, 18), we found that the hDRG neurons demonstrate a wide variety of evoked action potential firing patterns, with the majority falling under the single- and repetitive-spiking umbrellas. Segmentation based on firing phenotype revealed significant differences in the spike waveform, kinetics, and membrane properties between the single and repetitive clusters, suggesting that these two clusters are physiologically distinct from each other. These observations are also consistent with recent findings that report physiological clusters in hiPSC-derived sensory neurons and primary hDRG neurons obtained from organ donors(32).

We additionally identified a few cells (1/53 in the No Pain Hx group; 1/21 in the Pain Hx group) with a “burst-like” firing pattern in response to depolarizing current steps and anode break excitation. The firing pattern of these neurons, which show rapid adaptation and never fire more than two action potentials across all current steps tested (Figure 1), strongly resemble that of Aβ slow-adapting (SA) low-threshold mechanoreceptor (LTMR) population in mouse DRG (17). In

hDRG, putative Aβ SA LTMRs have been reported to be mostly large-diameter neurons with an average soma diameter of 89μm, albeit with broad distribution (minimum and maximum between approximately 25μm and 130μm; (11). Given that our study preferentially recorded from neurons with soma diameter <60μm, the large average diameter of the Aβ SA LTMRs may explain why only two cells included in our study (each with soma size of 43.6 μm, 27.9μm) displayed this burst-like firing pattern.

Different studies over time have reported different proportions of single- vs. repetitive-spiking clusters. For instance, one study using thoracic (T2-T12) DRG reported most dissociated hDRG neurons to be single spikers(46), while a study using lumbar (L1-L5) DRG have demonstrated that only ~ 25% of hDRG neurons exhibited the single-spiking phenotype under culture conditions(45). Our study, utilizing the T11-L5 DRG from human donors, found that the dissociated hDRG neurons were evenly distributed between the single- and repetitive-spiking clusters for both pain and non-pain groups. This may be due to differences in experimental conditions, such as levels of the DRG utilized, or differences in the delay between surgical extraction and culture.

Physiological specialization in transcriptionally distinct clusters of human sensory neurons

A previous study using mice with genetically labelled sensory neurons demonstrated that genetically distinct subpopulations of sensory neurons have markedly different firing patterns (17). Linking the electrophysiological and transcriptional phenotypes in hDRG poses unique challenges due to lack of readily available genetic labelling strategies, and the widespread distribution of nociceptors across multiple cell sizes. Utilizing the Patch-seq approach allowed us to circumvent these challenges and obtain both electrophysiological and transcriptional data from the same hDRG neuron.

We observed that transcriptionally identified clusters tend to be preferentially associated with one spiking phenotype, as seen in both *MRGPRD, CALCA+SSTR2,* and *CALCA+BMPR1B*

populations (Figure 2C). This is consistent with findings in mice, where different populations of sensory neurons exhibit 1 - 2 “characteristic” firing phenotype(17). The presence of both single- and repetitive-spiking population in the *MRGPRD* and *CALCA+BMPR1B* clusters suggests that single- and repetitive-spiking properties may reflect functional states of nociceptors that may be dynamically regulated by pain-inducing injury, as proposed previously(18). Indeed, recent work in hDRG has shown that persistent depolarization leads to changes in the relative representation of single and repetitively-firing neurons in both human and mouse DRG (45), suggesting that human sensory neurons can regulate their excitability and shift their spike firing patterns in response to external stimuli.

Our results provide proof-of-concept evidence that Patch-seq is a viable approach to map the transcriptionally defined neuronal phenotypes to electrophysiological characteristics defined by intrinsic excitability and other parameters in human neurons. Previously, Patch-seq has been used in the study of sensory neurons in rodent models (47) and human pluripotent stem cell-derived sensory neuron cultures (48). The data presented here represent an interim analysis of a planned larger effort to generate a large Patch-seq database of hDRG neurons that will eventually be used to compare sensory neuron characteristics within and across species. The dataset may provide additional predictive value to preclinical studies using cultured DRG neurons, as it may allow prediction of transcriptional/functional phenotype based on physiological markers. For example, it is possible that there are subtle physiological differences between the repetitive spikers belonging to different transcriptional subtypes that may be revealed with a larger and more adequately powered sample size. This type of detailed analysis of E-type relative to T-type represents a long-term goal of our NIH HEAL-Initiative-supported human tissue program (part of the PRECISION Human Pain Network) and will require hundreds of recordings collected over several years to know whether specific electrophysiological features of hDRG neurons can be used exclusively to identify the recorded cell type. At present, we suggest that adding Patch-seq

to recordings from human sensory neurons affords the opportunity to analyze physiological differences in genetically defined subsets of sensory neurons, reducing the impact of cell type heterogeneity and allowing for more direct comparisons of human sensory neuron biology to the cell-type-specific data collected from animal model studies.

Pain-associated differences in neuronal excitability.

To date, several electrophysiological analyses of dissociated hDRG neurons have been completed using samples obtained from cancer patients with or without neuropathic pain(28–30). Our finding that pain history is associated with greater action potential spiking frequency and lower rheobase in the repetitive-spiking cluster of hDRG neurons is in line with the conclusions of these studies (28–30), as well as reports in rodent models of pain (18, 23–27). While we did not see an increase in the number of neurons with spontaneous activity in samples from the Pain Hx group, this may be due to both the relative heterogeneity of the pain history of our donors, as well as the differing degrees of severity between cancer-associated neuropathic/reticular pain seen in previous studies and the joint pain and other forms of musculoskeletal pain seen in our donor pool.

Surprisingly, pain history was associated with reduced excitability in the single-spiking population, including increased rheobase and right-shifted input-output curve. In rats, the single-spiking “rapidly-accommodation” shows no change in spontaneous activity or excitability following pain-inducing spinal cord injury(18). However, recent studies have demonstrated that hDRG neurons can engage in homeostatic plasticity, reflected as reduced excitability in response to sustained depolarization or prolonged treatment with bradykinin(19, 45). Therefore, it is possible that single-spiking DRG neurons from donors experiencing persistent pain become less excitable over time as part of a homeostatic response. Our Patch-seq data also suggest that a minority of single spikers belongs to the A-delta low threshold mechanoreceptor (LTMR) population, which detects non-noxious stimuli (Figure 2). Hyposensitivity to innocuous tactile and thermal stimuli

has been previously reported in patients with chronic pain, including chronic low back pain, musculoskeletal pain, and neuropathic pain (49–51). While this has been primarily hypothesized to be a centrally mediated effect (52), our results raise the possibility that reduced excitability in non-nociceptive peripheral afferents may also contribute to this phenomenon, particularly for hypoesthesia in the pain dermatome.

In our study, we found that pain history was associated with significantly higher within-cell expression of *SCN9A* and *SCN10A*. In mice, NaV1.7, encoded by *SCN9A*, is enriched in the nociceptor subpopulation, promotes repetitive firing of action potentials, and is crucial to modulating the activation threshold of nociceptors (12, 29, 53–55). Upregulation of NaV1.7 expression and potentiation of NaV1.7-mediated current in the DRG were found in a rat model of chemotherapy-induced peripheral neuropathy (CIPN) (29) and in painful human neuromas (56), suggesting that levels of NaV1.7 may be dynamically regulated in chronic pain. Gain-of-function mutations in NaV1.7 have been identified in patients with hereditary painful neuropathies (55, 57, 58). Importantly, studies in cancer patients with and without radiculopathy suggest that the presence of neuropathic pain is associated with increased expression of *SCN9A* in hDRG (29). Our results are consistent with these previous findings; additionally, our data suggest that the association between pain history and NaV1.7 upregulation likely extends beyond the cancer pain population and may be found in chronic musculoskeletal pain.

NaV1.8, encoded by *SCN10A*, is highly enriched in nociceptors of both mice and humans (11, 12). NaV1.8 plays a critical role in peripheral sensitization associated with persistent pain (59–61). NaV1.8 is upregulated in the axons of rodent DRG neurons following nerve injury(62) and in the neuromas of patients with painful neuromas(56). Gain-of-function mutations and overexpression of *SCN10A* has been shown to promote hyperexcitability in rodent sensory neurons, whereas pharmacological blockade and genetic loss-of-function of NaV1.8 leads to attenuation of neuropathic and inflammatory pain and reduction in the excitability of DRG neurons

(59, 60, 63–68). The results of our studies further point towards an association with higher NaV1.8 expression and chronic or persistent pain. The association between increased *SCN10A* expression and pain history is particularly intriguing considering the recent FDA-approval of the NaV1.8 inhibitor, suzetrigine (VX-548), which reduces post-surgical pain compared to placebo, with comparable efficacy to hydrocodone/acetaminophen (69, 70). Detailed knowledge into how the properties of native human neurons are altered in the context of chronic pain conditions may reveal new insights that can inform specific therapeutic strategies tailored to various etiologies of pain.

Limitations of our study

In animal studies, experimental manipulation allows researchers to draw conclusions about directionality in the relationship between injury and neuronal hyperactivity. In contrast, we were not able to draw causative conclusions about the relationship between pain history and neuronal hyperactivity due to the observational, rather than experimental, nature of our study involving donor-obtained hDRG neurons. For example, we are not able to determine whether the increased levels of *SCN9A* and *SCN10A* were due to upregulation following the injury or inflammatory condition associated with the donor's pain experience; or whether the donors' DRG neurons already had higher expression of *SCN9A* and *SCN10A,* which then predisposed them to becoming hyperexcitable following inflammation or injury. Secondly, our dataset almost certainly contains neurons that do not innervate the dermatome of pain in our pain donors. While techniques such as retrograde tracing would allow greater degree of specificity in recording neurons that precisely innervate the affected limb or organ, such approaches are not yet widely available for use in human donors. As a result, some of the heterogeneity seen in our Pain Donor dataset may be reflective of the heterogeneity in the innervation pattern of recorded neurons. Third, the pain phenotype of our donors is mixed: while mostly musculoskeletal in nature, the donors' pain conditions included a wide range of regions and pathologies. This heterogeneity may contribute to the variability in the "Pain Hx" group. It is important to note, however, that the

heterogeneity in the pain history of our donor pool is reflective of the heterogeneity of pain phenotypes seen in the wider population of chronic pain patients(2). Finally, our samples contain limited demographic of the donors we had access to for this study. As a result of this limitation, there may be valuable physiological information related to sex or race that was not revealed in our study.

Summary and future directions

In summary, this study shows that human sensory neurons display a diverse array of electrophysiological phenotypes, which can be linked to specific transcriptionally defined subpopulations using Patch-seq. We additionally demonstrate that pain history of donors is associated with hyperexcitability in a subset of hDRG neurons and increased transcriptional expression of NaV1.7 and NaV1.8. Our study establishes Patch-seq as a useful tool in studying the biology and function of human sensory neurons, with ongoing efforts to generate a larger, publicly available Patch-seq database of hDRG neurons that can be used for future investigations. The findings and methodology presented in this study contributes to better understanding of cross-species differences in DRG neurons and provides further insights into pain-associated plasticity in sensory neurons that may inform therapeutic development in the future.

Methods

hDRG extraction

Extraction and collection of hDRGs were performed as previously described(71) in collaboration with Mid-American Transplant, with the following modifications and specifications. T11 - L5 DRGs were surgically removed from postmortem organ donors, within 1 -3 hours of aortic cross-clamping. Extracted DRGs were immediately placed in ice-cold, oxygenated N-methyl-D-glucamine (NMDG)-based artificial cerebrospinal fluid (aCSF; 93 mM NMDG, 2.5 mM KCl, 1.25 mM NaH_2PO_4, 30 mM $NaHCO_3$, 20 mM HEPES, 25 mM glucose, 5 mM ascorbic acid, 2 mM thiourea, 3 mM Na^+ pyruvate, 10 mM $MgSO_4$, 0.5 mM $CaCl_2$, 12 mM N-acetylcysteine; adjusted

to pH 7.3 using NMDG or HCl, and 300 - 310mOsm using H_2O or sucrose) and transported to lab for processing.

Donor inclusion and classification

Donors that were older than 60 years, had a body mass index greater than 40, or had positive serology for blood-borne diseases such as hepatitis C or human immunodeficiency virus (HIV) were excluded from the study. Donors' past medical history was determined using available information on the United Network of Organ Sharing (UNOS) documentation and Mid-America Transplant's interview with the donors' family members. A donor was classified as having significant pain history if they met two out of three of the following criteria: (a) the word "pain" is used to describe donor's recent or present medical condition (e.g., "daily pain," "regular pain," "painful tendonitis,"), and the dermatome of pain is specified to be in the back and/or the lower body; (b) donor's medical history includes prescribed use of analgesics (e.g., hydrocodone or gabapentin) that is unrelated to substance use disorder, or there is documentation of other non-pharmaceutical interventions for pain (e.g., back surgery, nerve blocks); (c) donor's medical history includes a disorder for which pain is a major symptom, such as arthritis or scleroderma. Based on these inclusion criteria, eight donors were identified as having a significant pain history ("Pain Hx"). Donors whose medical history did not mention any significant or possible pain conditions were classified as having no pain history (N = 10; "No Pain Hx"). Finally, six donors only partially met the above criteria for having a significant pain history, or had medical histories that included descriptions of possible pain-related conditions but lacked sufficient details to positively determine their pain statuses; and two donors had medical histories which included pain in areas that were non-lumbar dermatomes (e.g., migraine). These 8 donors were identified as possible confounds and excluded from further analysis. Demographic information and pain-related history of each donor is provided in Table 1.

hDRG primary culture

Primary culture of hDRGs were performed as previously described(45, 71). Briefly, 2 - 3 thoracolumbar DRGs were cleaned and finely minced using ice-cold NMDG-aCSF. Minced DRGs were sequentially dissociated using papain (Worthington, Lakewood NJ) and collagenase type 2 (Sigma-Aldrich, Darmstadt, Germany), then triturated for mechanical dissociation. Dissociated DRGs were filtered and resuspended in DRG media (5% fetal bovine serum [Gibco, Grand Island, NY], 1% penicillin/streptomycin [Corning, Corning, NY], Glutamax [Life Technologies, Carlsbad, CA), and B27 [Gibco] in Neurobasal-A [Gibco]). DRG was plated and cultured on collagen-coated glass coverslips, and media was changed every 2 - 3 days.

Patch-clamp electrophysiology

Patch-clamp experiments were performed between days in vitro (DIV) 2 - 8 (5.113 ± 1.484, average ± s.d.). Current clamp experiments were performed in external solution containing (in mM): 145 NaCl, 3 KCl, 2 $CaCl_2$, 1 $MgCl_2$, 7 glucose, 10 HEPES, adjusted to pH 7.3 with NaOH. Patch pipettes were pulled from thin-walled borosilicate glass with outer diameter of 1.5mm and internal diameter of 1.10mm (Sutter Instruments, Novato, CA). Pipettes were fire polished and had resistance values of 1 - 4 MΩ. The internal solution consisted of the following (in mM): 120 K-gluconate, 5 NaCl, 3 $MgCl_2$, 0.1 $CaCl_2$, 10 HEPES, 1.1 EGTA, 4 Na_2ATP, 0.4 Na_2GTP, 15 Na_2Phosphocreatine; adjusted to pH 7.3 with KOH and HCl, and 290 mOsm with sucrose. Patch-seq experiments were conducted with a modified K-gluconate internal designed to promote cDNA yield while maintaining electrophysiological properties, containing the following: 110 K-gluconate, 4 NaCl, 10 HEPES, 0.2 EGTA, 1 Na_2ATP, 0.3 Na_2GTP, 10 Na_2Phosphocreatine, 20 µg/mL glycogen, and 0.25 µL Protector RNAse Inhibitor; adjusted to pH 7.3 with KOH and HCl, and 290 mOsm with sucrose. Experiments were performed at room temperature. External solution was perfused continuously at a rate of 1 - 2 mL/min using a gravity-fed bath perfusion system. Recordings were made using a MultiClamp 700B amplifier, a Digidata 1550B digitizer, and the Clampfit software (v.11.1, Molecular Devices, San Jose, CA). All recordings were were sampled

at 10 kHz. Analysis of excitability, spike kinetics, and membrane properties was conducted using Easy Electrophysiology (Easy Electrophysiology Ltd., London, UK).

hDRG neurons with soma diameter < 60 μm were preferentially patched to increase the likelihood of recording from nociceptor populations(11). Membrane properties and excitability were measured in current clamp mode. After a stable whole-cell configuration was achieved and maintained for at least 2 minutes, a gap-free current-clamp recording was carried out for 1 - 2 minutes with no current injection in order to assess resting membrane potential and spontaneous activity. After the resting membrane potential was measured, hDRG neurons were held at -60 mV for assessment of membrane excitability and passive properties. Membrane excitability was determined using 1-s long stepwise current injections from 50 pA – 2 nA (Δ 50 pA). For any cells that did not fire at 2 nA, the current steps were extended until an action potential was elicited. Rheobase was defined as the minimum current injection required to trigger an action potential firing within the first 100 msec of the 1-second current step. To assess spike firing pattern, the number of action potential spikes fired in response to each current step was counted to generate an input-output curve for each cell. The action potential threshold was defined as the membrane voltage when dV/dt = 10 and was determined from the first action potential fired at rheobase. Action potential kinetics were measured using the first action potential fired at rheobase. Maximum rise and decay slopes were obtained from 10 - 90% of the rising and falling phases, respectively. Action potential half-width was defined as the time between 50% of the rising and falling phases. AP amplitude was measured from AP threshold to the peak of the spike. Input resistance was measured using hyperpolarizing current injections from -250 pA to -50 pA (Δ50 pA), by plotting ΔV_m against ΔI and determining the slope of the line of best fit. Voltage sag was measured using a single -250pA hyperpolarizing step. The magnitude of the sag was calculated as the difference between peak deflection and the steady-state V_m. The sag ratio was calculated by dividing the sag by the peak deflection magnitude. hDRG neurons with resting membrane

potential >30mV, or an unstable resting membrane potential, were considered to be unhealthy; recordings from those cells were excluded from analysis.

Cytosol Extraction

After the conclusion of whole-cell recording, cytosolic contents were aspirated into the recording pipet using gentle negative pressure for 2 - 3 minutes, until a visible shrinkage of the cell was observed (Supplementary Figure 3A). After aspiration, the recording pipette was slowly and gradually withdrawn. Contents of the patch pipette were immediately ejected into a sample collection tube containing 1 µL 10 x Reaction Buffer (95% Lysis Buffer [Takara Bio], 5% RNAse inhibitor [Takara Bio]), 8µL RT-PCR grade nuclease-free water (Thermo Scientific) by applying positive pressure. Samples made of Patch-seq internal solution were used as negative controls to assess ambient RNA contamination. Samples were stored at -80 °C for long-term storage. For Patch-seq experiments, experimenters were agnostic to the pain history status of the donors.

RNA sequencing of cytosolic contents

RNA was converted into cDNA using SMART-Seq® v4 Ultra® Low Input RNA Kit for Sequencing following the manufacture's manual. Samples containing 50 pg of total mouse brain RNA and samples made of nuclease-free water were used as positive and negative controls for library preparation, respectively. Twenty PCR cycles were used for cDNA amplification to increase yield. cDNAs were assayed using an Agilent TapeStation 4200. Samples containing less than 2 ng total cDNA or less than 35% of total cDNA in the size range of 500 – 6000 bp were deemed low quality and typically not sequenced. The cDNA libraries were then prepared for sequencing using the Illumina Nextera XT Library Preparation Kit following the manufacturer's manual. Resulting libraries were pooled and sequenced on an Illumina NovaSeq 6000 instrument targeting at least 500k reads per library. Sequencing reads were aligned to hg38 Reference genome and gene expression counts were generated.

Clustering of Patch-seq gene expression data

The counts table of Patch-seq samples was loaded into Seurat (V4.4.0) in R (V4.4.1) for quality control and gene expression analysis. Raw counts were scaled to 10,000 transcripts per nucleus using NormalizeData() and scaled for each gene using ScaleData() functions. Highly variable genes were identified and the top 20 principal components (PCs) were retrieved with RunPCA() using default parameters. UMAP coordinates were calculated using RunUMAP() and transcriptional clusters were identified using FindClusters(resolution=0.4) based on the top 20 PCs.

Differential expression and gene ontology analysis

Differential expression analysis between E-types was done using FindMarkers() in Seurat comparing the gene expression of Patch-seq samples annotated as single spikers to those annotated as repetitive firing during E-type analysis. Only genes that are significant (adjusted p value < 0.05) were reported. Gene Ontology (GO) analysis was performed using topGO (V2.40.0) in R. Differentially expressed genes described above were used as the input gene list and all genes with average expression >0.5 in the same cells are used as the background gene list. Genes were annotated for their biological process and GO terms with p value < 0.05 were reported.

RNAScope *in situ* hybridization

L1-L5 hDRGs were fixed in 4% paraformaldehyde at 4 °C overnight, cryopreserved in 30% sucrose, then flash-frozen in OCT. Fixed-frozen hDRG were cryosectioned at 12 µm and mounted on Superfrost Plus slides (Fisher, Pittsburgh, PA). Slides were stored at -20 °C or -80 °C with desiccant until further use. Immediately prior to RNAScope, hDRG sections were dehydrated using 50%, 70%, and 100% ethanol and treated with Protease IV and hydrogen peroxide (ACDBio, Minneapolis, MN). RNAscope was performed following manufacturer's protocol. The following probes from ACDBio were used: SCN9A (cat. no.562251), SCN10A (cat. no.406291), and SCN11A (cat. no.404791). For each experiment, the probe was paired to Opal 570 (1:1000; Akoya

Biosciences, Marlborough, MA). To reduce autofluorescence, TrueBlack® Autofluorescence Quencher (Biotium, Fremont, CA) was applied at the end of RNAScope following manufacturer protocol, either before or after the application of DAPI. Slides were mounted with coverslips using ProLong Gold Antifade Mountant (Invitrogen, Waltham, MA) and stored at -20 °C until imaging.

Imaging and image analysis

RNAScope slides were imaged using Leica DM6b system at 20 x magnification. For each slide, the entire hDRG section was imaged using the tile scan and merge feature of the using Leica Application Suite X (LAS-X, v.3.7, Leica Microsystems, Wetzlar, Germany). Acquisition settings were kept consistent across all slides and different experimental days. The following acquisition parameters were used: DAPI, 50 ms exposure, 2.1 gain, FIM 30%; L5, 300 ms exposure, 2.5 gain, FIM 55%; TXR, 500 ms exposure, 3.0 gain, FIM 55%. Segmentation and RNA expression analysis was completed using HALO AI™ and the Multiple IHC module of HALO® (Indica labs). Satellite glial cells were distinguished from neuronal cell bodies visually based on their unique morphology.

Statistics

All data were analyzed using GraphPad Prism 9 (GraphPad Software Inc, Boston, MA) and R (V4.4.1). To inform the use of appropriate statistical tests, normality of residuals and heteroscedasticity were assessed for each dataset using Shapiro-Wilk test and Brown-Forsythe test, respectively. To assess statistical differences across multiple groups, one-way ANOVAs with Tukey's post-hoc test, Kruskall-Willis test with Dunn's post-hoc test, or Brown-Forsythe ANOVA with Dunnett's T3 tests were performed. All post-hoc tests were performed with multiple comparison corrections. To assess differences between groups in the input-output curves, restricted maximum likelihood (REML) mixed effects analysis with Geisser-Greenhouse correction was used. PCA analysis and K-means clustering of electrophysiological data was conducted using R. All data are represented as mean ± SEM unless otherwise noted. Detailed statistics are reported in Supplementary Information.

Study approval

Extraction procedures were approved by Mid-America Transplant, and an Internal Review Board (IRB) waiver was obtained from the Human Research Protection Office at Washington University in St. Louis. hDRG samples were obtained from postmortem organ donors with the consent for tissue donation for research from family members.

Data availability

Data will be made available upon reasonable request.

Author contributions

JY and RWG designed the study. JY performed RNAscope experiments, analyzed the electrophysiology data, performed statistical analyses, prepared figures, and wrote the manuscript. JY, AJW, ZB, JDR, AJD, JNL, RK, and PG conducted the electrophysiology experiments. JY and AT analyzed the RNAScope data. LY processed Patch-seq samples, analyzed the sequencing data, and prepared relevant figures. JY, LY, AJW, ZB, JDR, RAS, AJD, RK, JMM, JNL, PG, AC, and MP acquired and processed human tissue samples and prepared primary cell culture utilized in the study. JL assisted in human tissue procurement. BC acquired funding and assisted in study design. RWG acquired funding and supervised the project. All authors contributed to manuscript editing and approval.

Acknowledgements

This work was supported by the American Heart Association (AHA) through the AHA Predoctoral Fellowship #828671 (JY) and by the National Institutes of Health (NIH) through the NIH HEAL Initiative under award number U19NS130607 (RWG), part of the PRECISION Human Pain Network. We thank the past and present members of the Gereau lab for their helpful comments; and Mid-America Transplant for their collaboration in tissue procurement. Finally, we thank the organ donors and their families, whose invaluable gift made this research possible.

References

1. Gureje O, et al. The relation between multiple pains and mental disorders: Results from the World Mental Health Surveys. *Pain*. 2008;135(1–2):82–91.

2. Rikard SM, et al. Chronic Pain Among Adults — United States, 2019–2021. *MMWR Morb Mortal Wkly Rep*. 2023;72(15):379–385.

3. Fayaz A, et al. Prevalence of chronic pain in the UK: A systematic review and meta-analysis of population studies. *BMJ Open*. 2016;6(6):e010364.

4. Ferreira ML, et al. Global, regional, and national burden of low back pain, 1990–2020, its attributable risk factors, and projections to 2050: a systematic analysis of the Global Burden of Disease Study 2021. *Lancet Rheumatol*. 2023;5(6):e316–e329.

5. Dey S, Vrooman BM. Alternatives to Opioids for Managing Pain. *StatPearls*. [published online ahead of print: September 27, 2022]. https://www.ncbi.nlm.nih.gov/books/NBK574543/. Accessed July 16, 2023.

6. Sheahan TD, et al. Metabotropic glutamate receptor 2/3 (mGluR2/3) activation suppresses TRPV1 sensitization in mouse, but not human, sensory neurons. *eNeuro*. 2018;5(2):412–429.

7. Davidson S, et al. Group II mGluRs suppress hyperexcitability in mouse and human nociceptors. *Pain*. 2016;157(9):2081–2088.

8. Ford ZK, et al. Cannabinoid Receptor 1 Expression in Human Dorsal Root Ganglia and CB13-Induced Bidirectional Modulation of Sensory Neuron Activity. *Frontiers in Pain Research*. 2021;2(November):1–9.

9. Slivicki RA, et al. The cannabinoid agonist CB-13 produces peripherally mediated analgesia in mice but elicits tolerance and signs of central nervous system activity with repeated dosing. *Pain*. 2022;163(8):1603–1621.

10. Shiers SI, et al. Convergence of peptidergic and non-peptidergic protein markers in the human dorsal root ganglion and spinal dorsal horn. *Journal of Comparative Neurology*. 2021;529(10):2771–2788.

11. Tavares-Ferreira D, et al. Spatial transcriptomics of dorsal root ganglia identifies molecular signatures of human nociceptors. *Sci Transl Med*. 2022;14(632):8186.

12. Shiers S, Klein RM, Price TJ. Quantitative differences in neuronal subpopulations between mouse and human dorsal root ganglia demonstrated with RNAscope in situ hybridization. *Pain*. 2020;161(10):2410–2424.

13. Wangzhou A, et al. Pharmacological target-focused transcriptomic analysis of native vs cultured human and mouse dorsal root ganglia. *Pain*. 2020;161(7):1497–1517.

14. Jung M, et al. Cross-species transcriptomic atlas of dorsal root ganglia reveals species-specific programs for sensory function. *Nat Commun*. 2023;14(1):366.

15. Zhang X, et al. Voltage-gated Na+ currents in human dorsal root ganglion neurons. *Elife*. 2017;6. https://doi.org/10.7554/eLife.23235.

16. Moy JK, et al. Distribution of functional opioid receptors in human dorsal root ganglion neurons. *Pain*. 2020;161(7):1636–1649.

17. Zheng Y, et al. Deep Sequencing of Somatosensory Neurons Reveals Molecular Determinants of Intrinsic Physiological Properties. *Neuron*. 2019;103(4):598-616.e7.

18. Odem MA, et al. Isolated nociceptors reveal multiple specializations for generating irregular ongoing activity associated with ongoing pain. *Pain*. 2018;159(11):2347–2362.

19. Yi J, et al. Bradykinin receptor expression and bradykinin-mediated sensitization of human sensory neurons. *bioRxiv*. 2023;2023.03.31.534820.

20. del Rosario J, et al. Sustained depolarization induces homeostatic plasticity in mouse and human sensory neurons. *2022 Neuroscience Meeting Planner.* San Diego, CA: Society for Neuroscience; 2022:Program No. 318.19.

21. Walters ET, et al. Persistent nociceptor hyperactivity as a painful evolutionary adaptation. *Trends Neurosci*. 2023;1–17.

22. Costigan M, Scholz J, Woolf CJ. Neuropathic Pain: A Maladaptive Response of the Nervous System to Damage. *Annu Rev Neurosci*. 2009;32(1):1–32.

23. Ma C, et al. Similar electrophysiological changes in axotomized and neighboring intact dorsal root ganglion neurons. *J Neurophysiol*. 2003;89(3):1588–1602.

24. Weng X, et al. Chronic inflammatory pain is associated with increased excitability and hyperpolarization-activated current (Ih) in C- but not Aδ-nociceptors. *Pain*. 2012;153(4):900–914.

25. Djouhri L, et al. Spontaneous pain, both neuropathic and inflammatory, is related to frequency of spontaneous firing in intact C-fiber nociceptors. *Journal of Neuroscience*. 2006;26(4):1281–1292.

26. Djouhri L, et al. Persistent hindlimb inflammation induces changes in activation properties of hyperpolarization-activated current (Ih) in rat C-fiber nociceptors in vivo. *Neuroscience*. 2015;301:121–133.

27. Serra J, et al. Microneurographic identification of spontaneous activity in C-nociceptors in neuropathic pain states in humans and rats. *Pain*. 2012;153(1):42–55.

28. North RY, et al. Electrophysiological Alterations Driving Pain-Associated Spontaneous Activity in Human Sensory Neuron Somata Parallel Alterations Described in Spontaneously Active Rodent Nociceptors. *Journal of Pain*. 2022;23(8):1343–1357.

29. Li Y, et al. DRG voltage-gated sodium channel 1.7 is upregulated in paclitaxel-induced neuropathy in rats and in humans with neuropathic pain. *Journal of Neuroscience*. 2018;38(5):1124–1136.

30. North RY, et al. Electrophysiological and transcriptomic correlates of neuropathic pain in human dorsal root ganglion neurons. *Brain*. 2019;142(5):1215–1226.

31. Namer B, et al. Specific changes in conduction velocity recovery cycles of single nociceptors in a patient with erythromelalgia with the I848T gain-of-function mutation of Na v 1.7. *Pain*. 2015;156(9):1637–1646.

32. Zurek NA, et al. Electrophysiological Analyses of Human Dorsal Root Ganglia and Human Induced Pluripotent Stem Cell-derived Sensory Neurons From Male and Female Donors. *Journal of Pain*. [published online ahead of print: 2023]. https://doi.org/10.1016/j.jpain.2023.12.008.

33. Cadwell CR, et al. Electrophysiological, transcriptomic and morphologic profiling of single neurons using Patch-seq. *Nat Biotechnol*. 2016;34(2):199–203.

34. Bhuiyan SA, et al. Harmonized cross-species cell atlases of trigeminal and dorsal root ganglia. *Sci Adv*. 2024;10(25). https://doi.org/10.1126/SCIADV.ADJ9173.

35. Yu H, et al. Single-Soma Deep RNA sequencing of Human DRG Neurons Reveals Novel Molecular and Cellular Mechanisms Underlying Somatosensation. *bioRxiv*. [published online ahead of print: 2023]. https://doi.org/doi.org/10.1101/2023.03.17.533207.

36. Nguyen MQ, et al. Single-nucleus transcriptomic analysis of human dorsal root ganglion neurons. *Elife*. 2021;10:1–21.

37. Avraham O, et al. Profiling the molecular signature of satellite glial cells at the single cell level reveals high similarities between rodents and humans. *Pain*. 2022;Publish Ah(00):2348–2364.

38. Sharma N, et al. The emergence of transcriptional identity in somatosensory neurons. *Nature*. 2020;577(7790):392–398.

39. Usoskin D, et al. Unbiased classification of sensory neuron types by large-scale single-cell RNA sequencing. *Nat Neurosci*. 2015;18(1):145–153.

40. Djouhri L, Lawson SN. Aβ-fiber nociceptive primary afferent neurons: A review of incidence and properties in relation to other afferent A-fiber neurons in mammals. *Brain Res Rev*. 2004;46(2):131–145.

41. Lawson SN, Fang X, Djouhri L. Nociceptor subtypes and their incidence in rat lumbar dorsal root ganglia (DRGs): focussing on C-polymodal nociceptors, Aβ-nociceptors, moderate pressure receptors and their receptive field depths. *Curr Opin Physiol*. 2019;11:125–146.

42. Yang L, et al. Human and mouse trigeminal ganglia cell atlas implicates multiple cell types in migraine. *Neuron*. 2022;1–16.

43. Kwan KY, et al. TRPA1 Contributes to Cold, Mechanical, and Chemical Nociception but Is Not Essential for Hair-Cell Transduction. *Neuron*. 2006;50(2):277–289.

44. Bandell M, et al. Noxious cold ion channel TRPA1 is activated by pungent compounds and bradykinin. *Neuron*. 2004;41(6):849–57.

45. McIlvried LA, et al. Intrinsic adaptive plasticity in mouse and human sensory neurons. *J Gen Physiol*. 2024;157(1):e202313488.

46. Davidson S, et al. Human sensory neurons: Membrane properties and sensitization by inflammatory mediators. *Pain*. 2014;155(9):1861–1870.

47. Parpaite T, et al. Patch-seq of mouse DRG neurons reveals candidate genes for specific mechanosensory functions. *Cell Rep*. 2021;37(5). https://doi.org/10.1016/j.celrep.2021.109914.

48. Truong V, et al. Transcriptomic analysis and high throughput functional characterization of human induced pluripotent stem cell derived sensory neurons. *bioRxiv*. 2024;2024.08.23.607310.

49. Puta C, et al. Somatosensory Abnormalities for Painful and Innocuous Stimuli at the Back and at a Site Distinct from the Region of Pain in Chronic Back Pain Patients. *PLoS One*. 2013;8(3):e58885.

50. Nathan PW. Improvement in cutaneous sensibility associated with relief of pain. *J Neurol Neurosurg Psychiatry*. 1960;23(3):202–206.

51. Marchettini P, et al. Lidocaine test in neuralgia. *Pain*. 1992;48(3):377–382.

52. Moriwaki K, Yuge O. Topographical features of cutaneous tactile hypoesthetic and hyperesthetic abnormalities in chronic pain. *Pain*. 1999;81(1–2):1–6.

53. Djouhri L, et al. Sensory and electrophysiological properties of guinea-pig sensory neurones expressing Nav 1.7 (PN1) Na+ channel α subunit protein. *Journal of Physiology*. 2003;546(2):565–576.

54. Dib-Hajj SD, et al. The Na v 1.7 sodium channel: From molecule to man. *Nat Rev Neurosci*. 2013;14(1):49–62.

55. Faber CG, et al. Gain of function Na V1.7 mutations in idiopathic small fiber neuropathy. *Ann Neurol*. 2012;71(1):26–39.

56. Black JA, et al. Multiple sodium channel isoforms and mitogen-activated protein kinases are present in painful human neuromas. *Ann Neurol*. 2008;64(6):644–653.

57. Yang Y, et al. Nav1.7-A1632G Mutation from a Family with Inherited Erythromelalgia: Enhanced Firing of Dorsal Root Ganglia Neurons Evoked by Thermal Stimuli. *The Journal of Neuroscience*. 2016;36(28):7511.

58. Ghovanloo MR, et al. Nav1.7 P610T mutation in two siblings with persistent ocular pain after corneal axon transection: impaired slow inactivation and hyperexcitable trigeminal neurons. *J Neurophysiol*. 2023;129(3):609–618.

59. Payne CE, et al. A novel selective and orally bioavailable Nav1.8 channel blocker, PF-01247324, attenuates nociception and sensory neuron excitability. *Br J Pharmacol*. 2015;172(10):2654–2670.

60. Zhang XF, et al. A-887826 is a structurally novel, potent and voltage-dependent Nav1.8 sodium channel blocker that attenuates neuropathic tactile allodynia in rats. *Neuropharmacology*. 2010;59(3):201–207.

61. Kort ME, et al. Subtype-selective Nav1.8 sodium channel blockers: Identification of potent, orally active nicotinamide derivatives. *Bioorg Med Chem Lett*. 2010;20(22):6812–6815.

62. Gold MS, et al. Redistribution of Nav1.8 in uninjured axons enables neuropathic pain. *Journal of Neuroscience*. 2003;23(1):158–166.

63. Jarvis MF, et al. A-803467, a potent and selective Nav1.8 sodium channel blocker, attenuates neuropathic and inflammatory pain in the rat. *Proc Natl Acad Sci U S A*. 2007;104(20):8520–8525.

64. Faber CG, et al. Gain-of-function Nav1.8 mutations in painful neuropathy. *Proc Natl Acad Sci U S A*. 2012;109(47):19444–19449.

65. Han C, et al. The G1662S NaV1.8 mutation in small fibre neuropathy: Impaired inactivation underlying DRG neuron hyperexcitability. *J Neurol Neurosurg Psychiatry*. 2014;85(5):499–505.

66. Han C, et al. Human Nav1.8: Enhanced persistent and ramp currents contribute to distinct firing properties of human DRG neurons. *J Neurophysiol*. 2015;113(9):3172–3185.

67. Huang J, et al. Small-fiber neuropathy Nav1.8 mutation shifts activation to hyperpolarized potentials and increases excitability of dorsal root ganglion neurons. *Journal of Neuroscience*. 2013;33(35):14087–14097.

68. Xiao Y, et al. Increased resurgent sodium currents in nav1.8 contribute to nociceptive sensory neuron hyperexcitability associated with peripheral neuropathies. *Journal of Neuroscience*. 2019;39(8):1539–1550.

69. Vertex Announces Positive Results From the VX-548 Phase 3 Program for the Treatment of Moderate-to-Severe Acute Pain | Vertex Pharmaceuticals [Internet]. *Vertex Press Release*. 2024. https://investors.vrtx.com/news-releases/news-release-details/vertex-announces-positive-results-vx-548-phase-3-program. Accessed March 6, 2025.

70. Jones J, et al. Selective Inhibition of Na V 1.8 with VX-548 for Acute Pain . *New England Journal of Medicine*. 2023;389(5):393–405.

71. Valtcheva M V., et al. Surgical extraction of human dorsal root ganglia from organ donors and preparation of primary sensory neuron cultures. *Nat Protoc*. 2016;11(10):1877–1888.

Table 1. Demographic information and pain-related history of donors included in the study.

Age	Sex	Race	BMI	COD	Pain Hx	Number of cells patched	Inclusion in RNAScope
No pain history							
53	M	White	30.3	Anoxia	None	2	x
51	F	White	33.5	Anoxia	None	3	
12	M	White	20.0	Anoxia	None	1	
45	M	White	28.8	Anoxia	None	0	x
23	M	White	14.3	Head trauma	None	4	
23	F	White	35.4	Head trauma	None	9	
17	M	Black	22.6	Anoxia	None	2	x
50	F	White	25.4	Anoxia	None	0	x
56	F	Black	25.0	Stroke	None	0	x
31	M	White	21.6	Anoxia	None	6	
31	M	White	31.6	Anoxia	Dental pain in 2018; no present pain condition or prescription pain medication noted.	4	
32	M	White	28.8	Anoxia	None	3	
33	M	White	34.0	Stroke	None	14	
38	f	black	28.3	Stroke	None	1	
43	f	white	19.8	stroke	None	3	
58	m	black	19.7	stroke	None	5	
53	f	white	33.0	stroke	None	7	
Pain hx							
23	M	White	26.4	Head trauma	Constant joint pain since age 17	0	x
56	F	Black	23.1	Anoxia	Leg pain and scleraderma. Regular use of prescription pain medication.	2	
53	M	White	24.2	Stroke	History of multiple back surgeries, arthritis, bulging disc, back injury. Used prescribed pain medication for >5 years.	3	
53	M	Black	36.5	Anoxia	Knee pain due to arthritis	1	
26	M	Black	37.8	Anoxia	Knee pain due to tendonitis from playing football	1	
59	M	White	33.6	Anoxia	Arthritis; history of knee surgery and prospective hip replacement surgery.	1	x
58	F	Unknown	34.1	Stroke	Degenerative disk disease; nerve block injections for back pain.	2	x
59	M	White	35.6	Stroke	Arthritis; prescribed pain medication	7	
52	F	White	22.4	Stroke	Severe pain in the groin, leading to difficulty walking. Occasional migraines and neck pain	1	
Confound: uncertain pain history							
53	M	White	39.6	Stroke	"Chronic inflammation" of the back managed with OTC[1] ibuprofen	5	
42	M	White	29.9	Head trauma	Gunshot wound to the leg that led to difficulty walking at times.	2	
60	M	White	32.4	Anoxia	Prior history of disc replacement, possibly cervical. Reason for disc replacement was not provided.	2	

49	F	White	19.25	Anoxia	IV vicodin, heroin use history; recurrent kidney stones	2	
48	M	White	38.16	Head trauma	Hx diabetes with right below-knee amputation; home med list includes gabapentin and hydrocodone-acetaminophen but no explicit neuropathy or pain mentioned	4	
61	m	white	26.57	stroke	Home med list includes oxycodone. History of diabetes and upper limb ischemia, but no neuropathy or pain mentioned	1	
Confound: pain in non-lumbar dermatomes							
32	M	White	30.7	Head trauma	Frequent joint pain in hand and thumb from a prior injury	2	x
39	M	White	24.1	Head trauma	Regular and severe headaches managed with OTC NSAIDs[2] and acetaminophen. Possible pediatric rheumatoid disease.	6	x

[1]OTC, over-the-counter; NSAID, nonsteroidal anti-inflammatory drug.

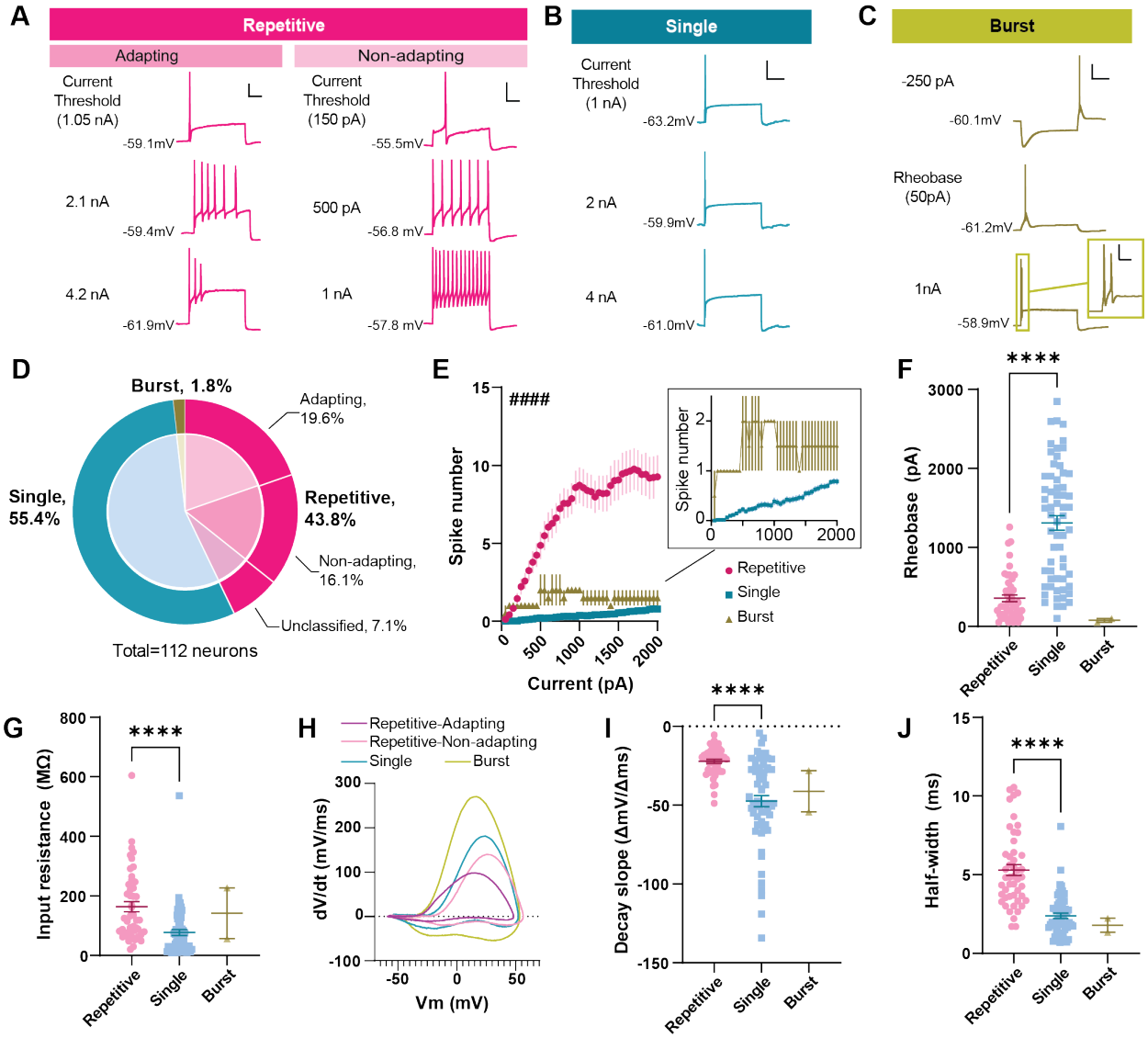

Figure 1. Physiologically distinct clusters of human sensory neurons. (A) Sample traces of repetitive firing neurons. Left, sample trace of action potential firing pattern from a hDRG neuron that displays spike frequency adaptation in response to suprathreshold current injections. Right, sample trace of spike firing pattern from a hDRG neuron that does not display spike frequency adaptation. (B) Sample trace of a single-spiking neuron at rheobase and at suprathreshold current injections. (C) Sample trace of a burst-like firing hDRG neuron characterized by anode-break excitation and burst-like action potentials. (A-C) Scale bars, 25mV/250ms. (D) Relative distribution of each firing phenotype. (E) Input-output curve of the four different physiological clusters. Inset: zoomed in plot showing the input-output curves of single- and burst-like phenotypes. ####, $p < 0.0001$, fixed effect of interaction between firing phenotype and current injection, mixed-effects analysis. (F) Number of action potentials fired in response to suprathreshold current injection at 2x rheobase. (G-I) Membrane properties across the four phenotypes, including rheobase (G), input resistance (H), and voltage sag (I). (J) Sample phase-plots of representative neurons from the four clusters. (K) Maximum kinetic properties and (L) Half-width of the first action potential at rheobase. *$p < 0.05$, **$p < 0.01$, ***$p < 0.001$, ****$p < 0.0001$; Dunn's (F, H, I) or Dunnett's T3 (G, K, L) post-hoc test following Kruskal-Wallis test, one-way ANOVA, or Brown-Forsythe ANOVA, respectively.

Table 2. Membrane properties and kinetics of E-types of human sensory neurons

	Repetitive (n=48)	Single (n=62)	Burst (n=2)
Diameter (μm)	35.81 ± 0.93	37.97 ± 1.86	35.75 ± 7.85
Resting membrane potential (mV)	-54.73 ± 1.94	-54.73 ± 1.07	-47.20 ± 1.29
Input resistance (MΩ)****	163.75 ± 17.03	77.00 ± 10.00	141.73 ± 85.41
Voltage sag ratio	0.3385 ± 0.0228	0.3849 ± 0.0232	0.6080 ± 0.0376
Rheobase (pA)****	356.51 ± 42.07	1308.82 ± 93.66	75.04 ± 24.71
AP threshold (mV)	-17.17 ± 1.44	-17.92 ± 1.43	-28.20 ± 0.61
AP Amplitude (mV)	69.70 ± 1.72	62.23 ± 2.77	78.42 ± 3.56
AP Overshoot (mV)*	52.18 ± 1.07	44.65 ± 2.04	50.22 ± 2.95
Half-width (ms)****	5.30 ± 0.34	2.38 ± 0.17	1.79 ± 0.44
Max rise slope (mV/ms)	126.71 ± 8.39	149.24 ± 13.91	227.66 ± 42.73
Max decay slope (mV/ms)****	-22.18 ± 1.27	-47.46 ± 3.50	-41.20 ± 13.12

*$p<0.05$, ****$p<0.0001$; Mann-Whitney test, Repetitive vs. Single

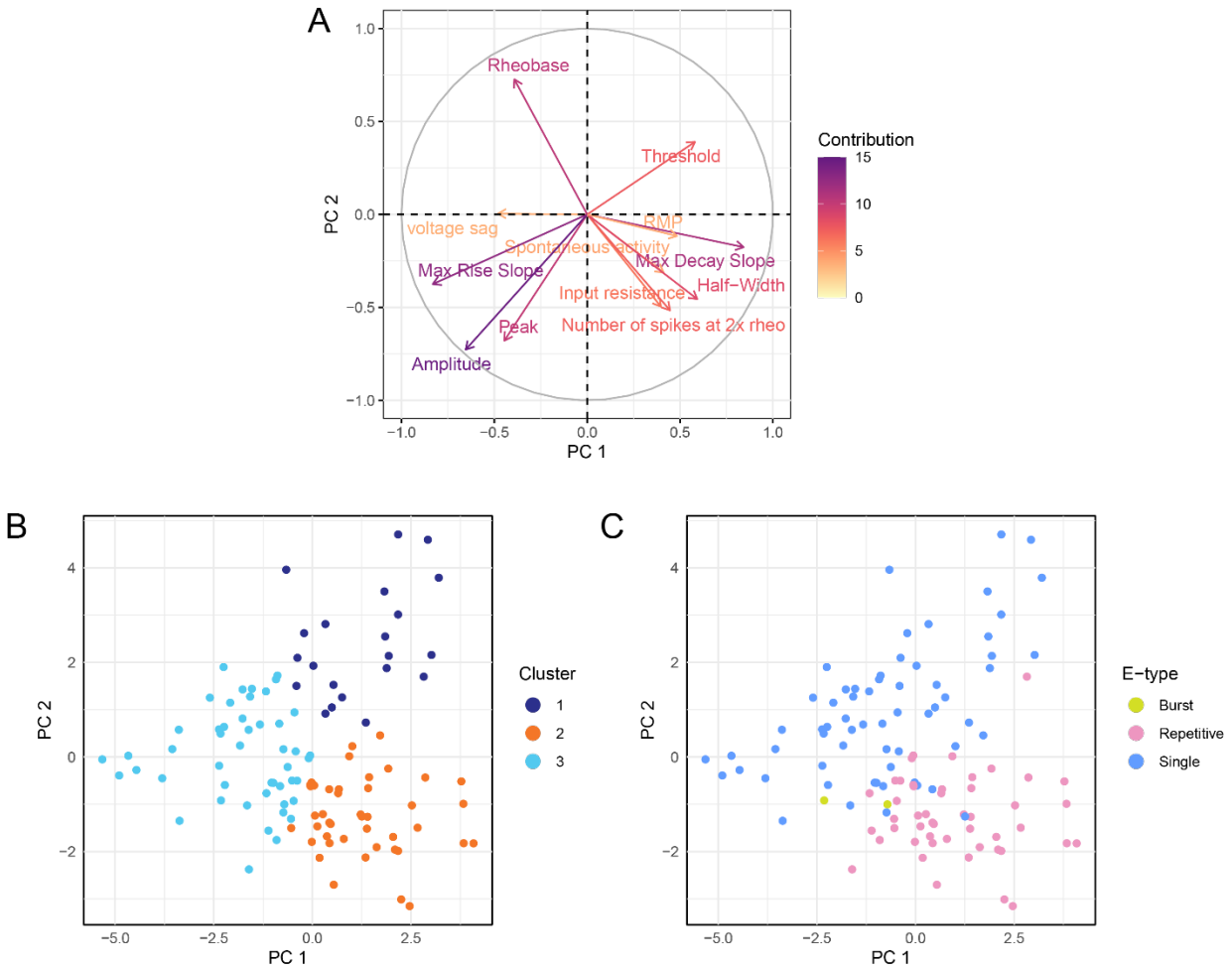

Figure 2. Principal component analysis (PCA) of the electrophysiological features from human sensory neurons. (A) Loading plot of PC1 and PC2 showing the relative contribution of each variable to each PCs. Membrane properties and spike kinetic parameters were used as variables for PCA. Membrane properties included input resistance, resting membrane potential (RMP), voltage sag, rheobase, spike threshold, and number of spikes fired at suprathreshold thresholds (defined as 2x rheobase). Spike kinetic parameters included in the analysis are spike amplitude, peak, rise slope, decay slope, and half-width. (B) Score plot of the hDRG neurons, clustered into three groups based on their electrophysiological properties. (C) Score plot of the hDRG neurons, grouped by their firing pattern as in Figure 1. The majority (90.3%) of single-firing neurons were split between Cluster 3 (36/62, or 58.1%) and Cluster 1 (20/62, or 32.2%). The majority of repetitive-firing neurons (37/48, or 77.1%) were found in Cluster 2; a subset (10/48, or 20.8%) of repetitive-firing neurons were correspond to Cluster 3. Both burst firing neurons (2/2) in our dataset belong to Cluster 3.

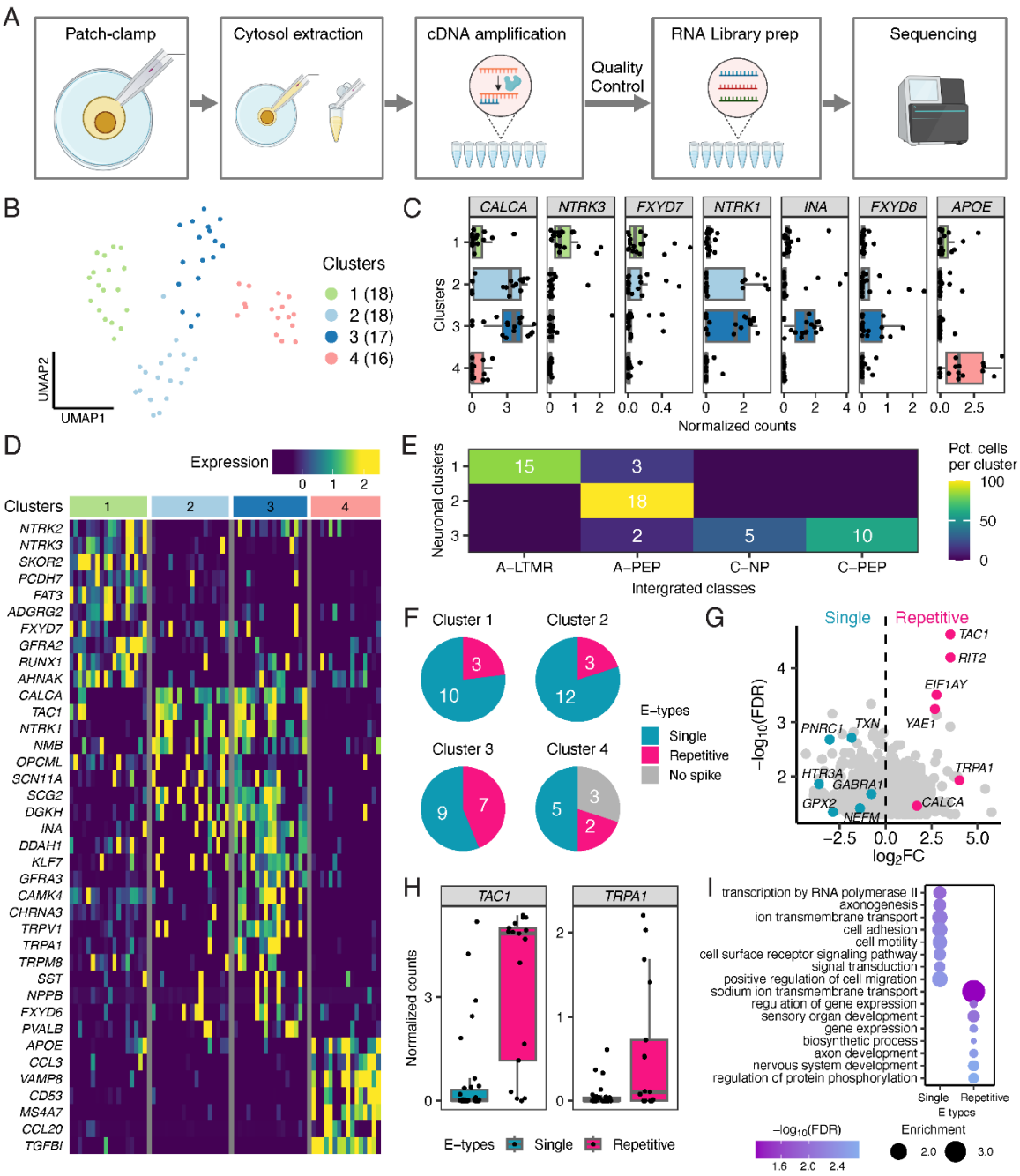

Figure 3. Using patch-seq to link electrophysiologically defined human DRG types to transcriptionally defined clusters. (A) Workflow of Patch-seq on cultured human DRG sensory neurons. (B) Uniform Manifold Approximation and Projection (UMAP) plot of 69 human DRG Patch-seq samples. Samples are colored by transcriptional clusters, and the numbers in the parentheses indicate cell counts in each cluster. (C). Normalized counts (log_2 transformed counts per million[log_2CPM]) of select human DRG cell class marker genes in each cluster. Scatter plot indicats the expression in individual samples and the boxes indicate quartiles and whiskers are 1.5-times the interquartile range (Q1-Q3). The median is a grey line inside each box. (D) Heatmap showing the scaled expression (Z-score of log_2CPM) of select marker genes from each transcriptional cluster in Patch-seq data. (E) Heatmap showing the percent (as the color gradient) and counts (as numbers on the heatmap) of samples in each transcriptional neuronal

cluster (clusters 1-3) that are assgined to the four cell classes identified in single-soma RNA-seq by integration. (F) Pie chart showing the distribution of E-types in each transcriptional cluster. (G) Volcano plot showing differentially expressed (DE) genes (FDR<0.05) in single- and repetitive- spiking neurons. Selected DE genes are labeled. (H) Box plot showing the expression of DE genes *TAC1* and *TRPA1* in single- and repetitive- spiking neurons. Scatter plot indicats the expression in individual samples and the boxes indicate quartiles and whiskers are 1.5-times the interquartile range (Q1-Q3). The median is a grey line inside each box. (I) Enriched gene ontology terms (p<0.05, enrichment > 1.5) in single- and repetitive- spiking neurons.

Repetitive spikers

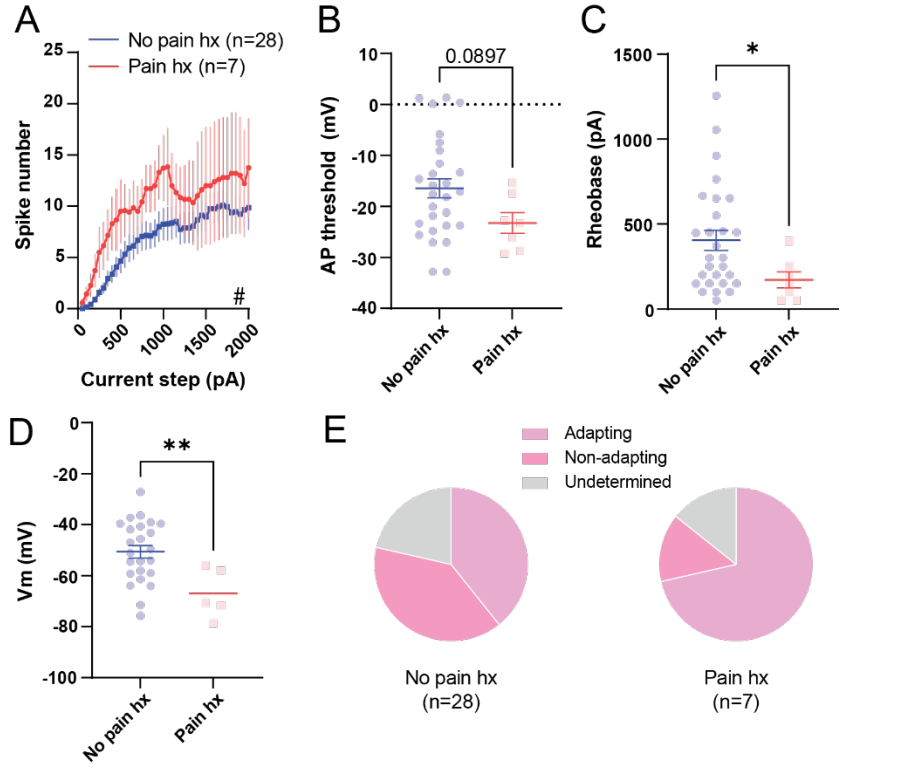

Single spikers

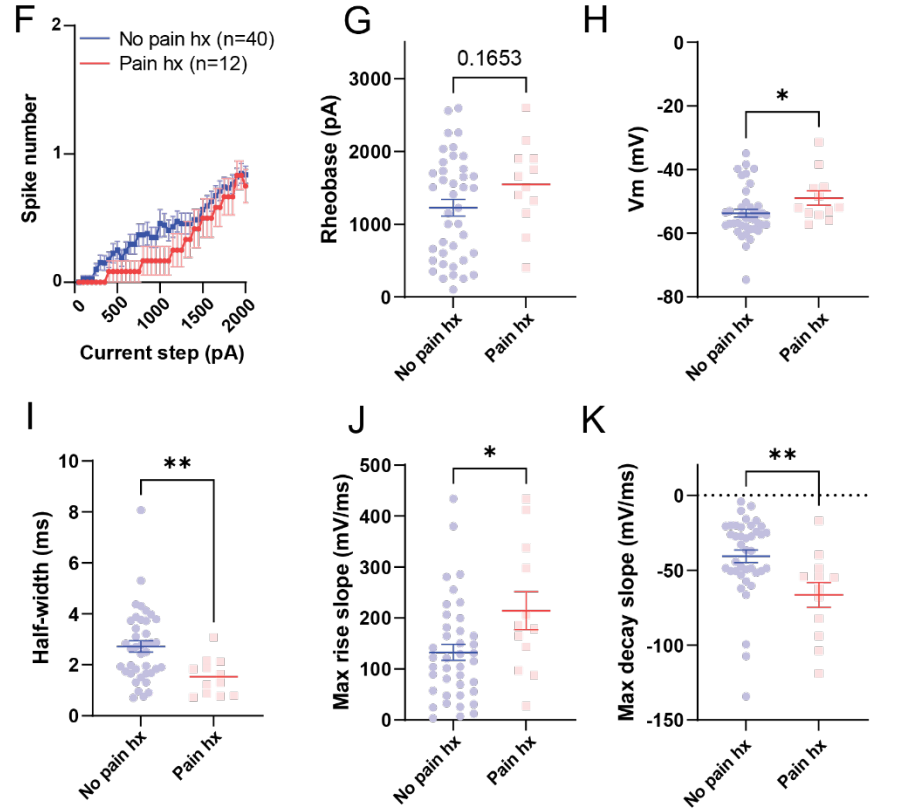

Figure 4. Pain history is associated with increased membrane excitability in repetitive spikers. (A) Input-output curve of repetitive spikers from donors with no pain history (blue) and documented pain history (red). $^{\#}p < 0.05$; mixed-effects analysis, fixed effect of pain history. (B) The voltage threshold for action potential was lower in repetitive neurons from pain donors compared to neurons from non-pain donors, with the difference approaching significance (unpaired t-test). (C-D) Rheobase (C) and resting membrane potential (D) were significantly different between groups. $^{*}p < 0.05$, $^{**}p<0.01$; Mann-Whitney test (C) and unpaired t-test (D). (E) Relative distributions of adapting and non-adapting repetitive spiking subtypes in neurons from donors without pain history (No Pain Hx; 39.3% adapting, 39.3% non-adapting, 21.4% undetermined) and donors with pain history (Pain Hx; 71.4% adapting, 14.3% non-adapting, 14.3% undetermined). (F) Input-output curve of single spikers from donors with no pain history (blue) and documented pain history (red). (G) There is no significant difference in the rheobase of single spikers from pain and non-pain donors (unpaired t-test). (H) Resting membrane potential is significantly more depolarized in single spikers from donors with pain history. (I-K) Spike kinetics in single spikers, including half-width (I), maximum rise slope (J), and maximum decay slope, are significantly different between pain and non-pain donors. $^{*}p < 0.05$, $^{**}p < 0.01$, Mann-Whitney test (H-K).

Table 3. Distribution of repetitive, single, and burst-firing neurons across different donor groups

	Repetitive	**Single**	**Burst**
No pain hx (n = 57)	28 (39.1%)	41 (59.4%)	1 (1.4%)
Pain hx (n = 21)	7 (35.0%)	12 (60.0%)	1 (5.0%)

Table 4. Membrane properties of hDRG neurons from donors with and without pain history.

	Repetitive			Single		
	No pain hx (n = 27)	Pain hx (n = 7)	p-value	No pain hx (n = 40)	Pain hx (n = 12)	p-value
Diameter (μm)	36.72 ± 1.15	33.13 ± 2.45	p = 0.1732	39.86 ± 2.45	34.68 ± 4.17	p = 0.2054
Resting membrane potential (mV)	-50.99± 2.54	-66.97 ± 4.33	**#p = 0.0109**	-53.69 ± 1.24	-48.94 ± 2.21	***p = 0.0311**
Input resistance (MΩ)	155.44 ± 25.81	186.12 ± 36.25	p = 0.2565	83.04 ± 14.45	54.64 ± 15.92	p = 0.1269
Voltage sag ratio	0.31 ± 0.03	0.40 ± 0.04	p = 0.1655	0.39 ± 0.03	0.41 ± 0.07	p = 0.5126
Rheobase (pA)	391.50 ± 59.27	172.07 ± 47.47	***p = 0.0435**	1226.12 ± 113.09	1545.96 ± 170.95	p = 0.1653
AP threshold (mV)	-16.39± 1.93	-23.25 ± 2.02	p = 0.0928	-17.09 ± 1.81	-19.43± 288.	p = 0.5284
AP Amplitude (mV)	66.41 ± 2.57	75.10 ± 2.77	p = 0.1067	60.45 ± 3.50	69.90 ± 4.81	p = 0.1383
AP Overshoot (mV)	50.02 ± 1.49	51.85 ± 2.156	p = 0.5633	43.37 ± 2.53	52.24 ± 1.72	***p = 0.0455**
Half-width (ms)	5.93 ± 0.51	5.38 ± 0.67	p = 0.8351	2.72 ± 0.22	1.53 ± 0.21**	****p = 0.0028**
Max rise slope (mV/ms)	117.0 ± 11.16	141.7 ± 21.52	p = 0.3205	132.48 ± 15.64	214.39 ± 37.29*	***p = 0.0364**
Max decay slope (mV/ms)	-20.71 ± 1.78	-20.58 ± 1.511	p = 0.8429	-40.77 ± 4.24	-66.53 ± 8.29*	****p = 0.0028**

*p < 0.05, Mann-Whitney test; #p<0.05, unpaired t-test; **p < 0.01, Mann-Whitney test

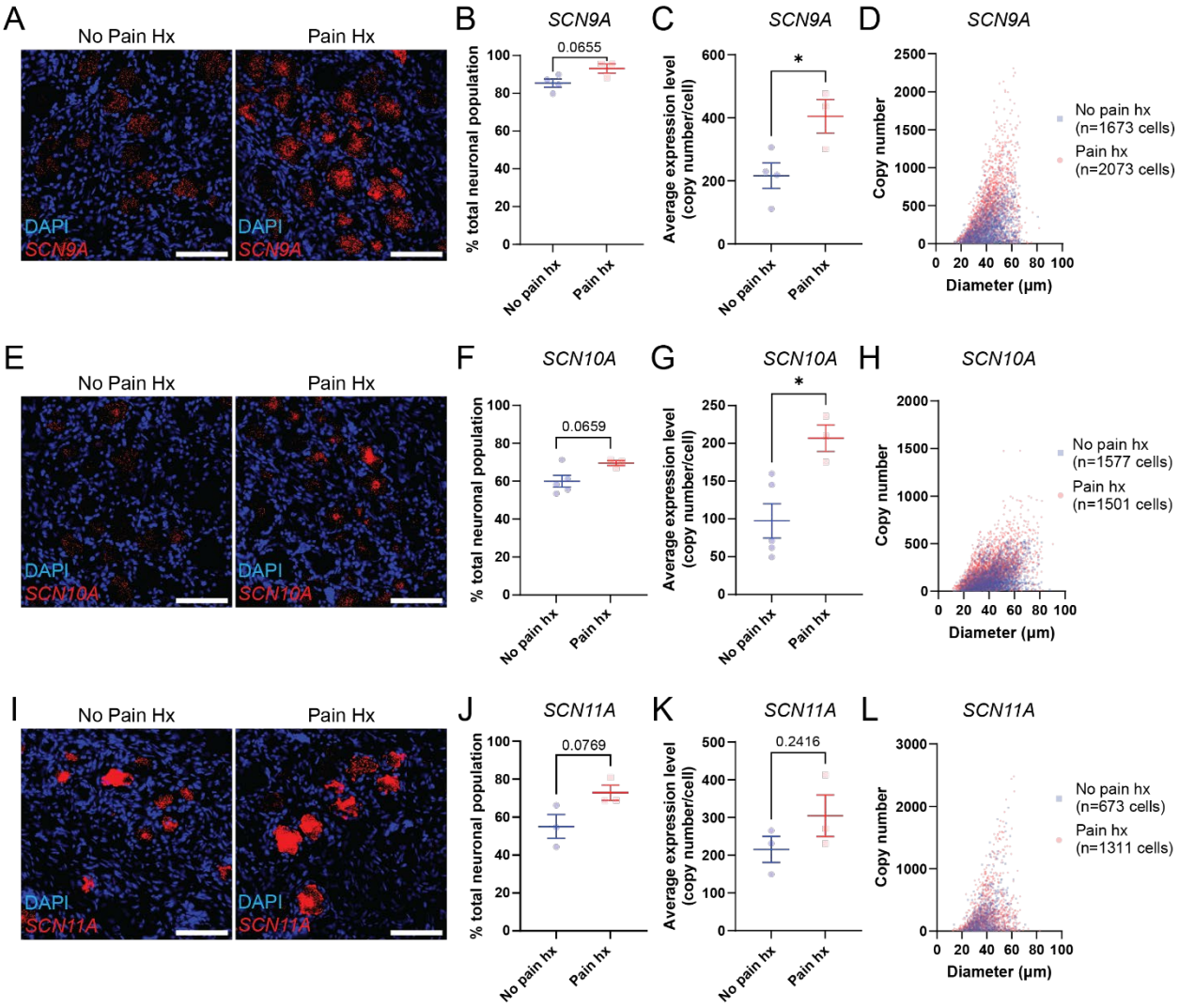

Figure 5. Donors with pain history exhibit higher levels of *SCN9A* and *SCN10A* expression than donors without pain history. (A) Representative images of DRG sections from donors with (right) and without (left) significant history of pain. RNAScope was performed for *SCN9A* (red), which encodes NaV1.7. Scale bar = 100µm. (B) Pain donors trended towards having a greater proportion of *SCN9A*+ DRG neurons compared to donors without pain history. Number of *SCN9A*+ neurons in the DRG was normalized to total number of neurons in the DRG for each donor. Comparison between groups showed that DRGs from pain donors tended to have higher proportions of *SCN9A*+ neurons, with the p-value approaching statistical significance. (C) Average within-cell expression of *SCN9A* is significanty higher in pain donors compared to donors with no pain history. For each donor, the *SCN9A* copy numbers of all *SCN9A*-expressing neurons were averaged (3 - 4 donors per group, 331-946 *SCN9A*+ cells per donor). Comparison between donors with and without a history of pain showed that *SCN9A*+ neurons from pain donors, on average, had higher levels of *SCN9A* transcripts compared to *SCN9A*+ neurons from non-pain donors. *$p < 0.05$, unpaired t-test. (D) Plot showing the *SCN9A* expression level in each neuron plotted against its soma size; neurons from pain donors are plotted in red, and neurons from donors without pain history are shown here in blue. Higher levels of *SCN9A* expression is seen across a broad range of soma sizes in pain donors. (E) Representative images of DRG sections from donors with (right) and without (left) significant history of pain. RNAScope was performed for *SCN10A* (red), which encodes NaV1.8. Scale bar = 100µm. (F) Pain donors trended towards having greater proportions of *SCN10A*+ DRG neurons compared to donors without pain history, with p-value approaching significance. (G) Average within-cell

expression of *SCN10A* is significanty higher in pain donors compared to donors with no pain history. Comparison between donors with and without a history of pain showed that *SCN10A*+ neurons from pain donors, on average, had higher levels of *SCN10A* transcripts compared to *SCN10A*+ neurons from non-pain donors (3 - 5 donors per group, 134-627 *SCN10A*+ cells per donor). *$p < 0.05$, unpaired t-test. (H) Higher levels of *SCN10A* expression is seen across a broad range of soma sizes in pain donors. (I) Representative images of DRG sections from donors with (right) and without (left) significant history of pain. RNAScope was performed for *SCN11A* (red), which encodes NaV1.9. Scale bar = 100µm. (J) Pain donors trended towards having greater proportions of *SCN10A*+ DRG neurons compared to donors without pain history . (K) There is no significant difference in the average within-cell expression of *SCN11A* in pain donors and donors with no pain history (3 donors per group, 175-719 *SCN11A*+ cells per donor). (L) *SCN11A* expression of every *SCN11A*+ cell plotted against its soma size.

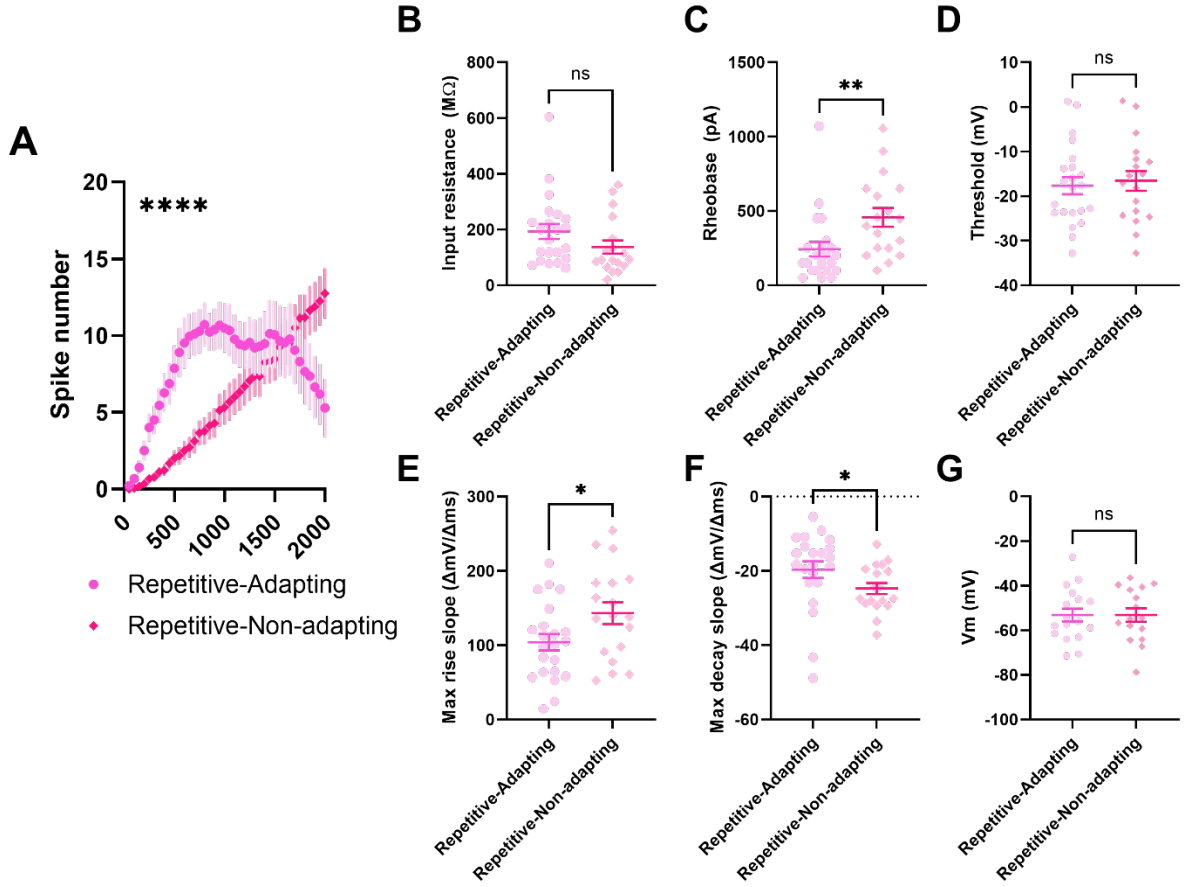

Supplementary Figure 1. Repetitive spikers of hDRG can be subdivided by presence of spike frequency adaptation. (A) Input-output curve plotting the number of action potential spikes fired against the amount of current injected. Repetitive-adapting subtype display an “inverse-U” input-output curve and reaches the maximal spike firing at lower current steps. The non-adapting subtype displays a linear input-output relationship. ****p<0.0001; mixed-effects analysis, fixed effect of the interaction of current step x subtype. (B-G) Comparison of membrane and spike kinetic properties between the two subtypes. Input resistance (B), voltage threshold for action potential firing (D), and resting membrane potential (G) are not significantly different between the two subtypes. Repetitive-adapting subtype has lower rheobase (C) than the non-adapting subtype, suggestive of greater excitability. The non-adapting subtype has faster spike kinetics than the adapting subtype, including the maximum rise (E) and decay (F) slopes. Ns = not significant, *p<0.05, **p<0.01; unpaired t-test (D, E, G) and Mann-Whitney test (B, C, F).

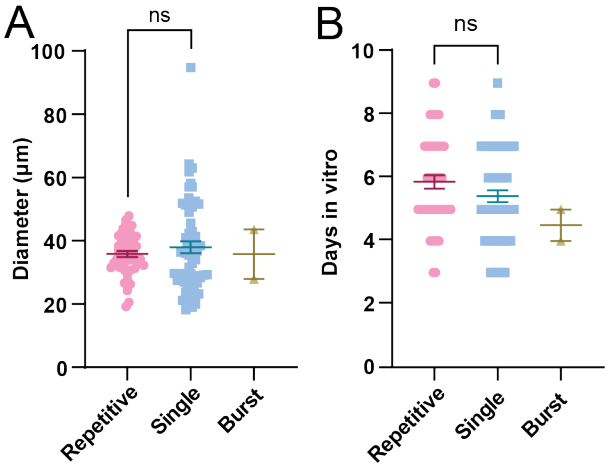

Supplementary figure 2. Cell size and number of days in culture are not significantly different across physiologically distinct clusters of human sensory neurons. (A) Distribution of cell size across the four different phenotypes. (B) Distribution of the number of days in culture prior to recording for each of the physiological cluster.

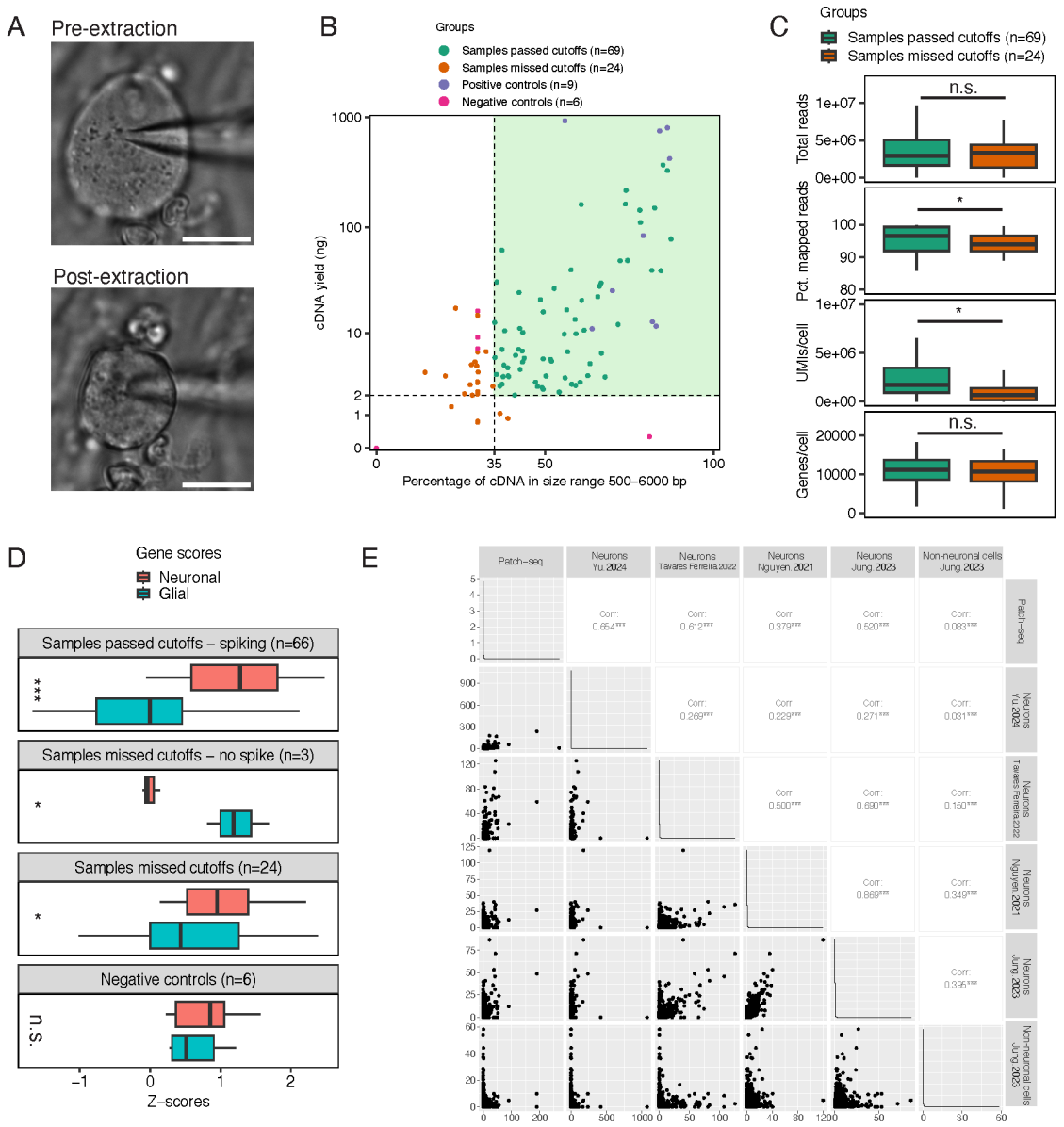

Supplementary figure 3. Quality control of Patch-seq data. (A) Example images of cytosolic content extraction from a recorded neuron. Shrinkage of the soma size can be visually confirmed during the extraction process. Scale bar = 30 um. (B) QC metrics of the cDNA library prepared from Patch-seq samples. Samples with cDNA yield > 2 ng and at least 35% of cDNA within the size range 500 -6000 bp are considered as high quality and proceed to library preparation and sequencing. Positive controls are prepared from 20 - 50 ng of total mouse brain RNA. Negative controls are prepared from either internal solution or nuclease-free water. (C) Sequencing metrics of the Patch-seq samples that passed the cDNA QC compared to the ones that failed QC. (D) Box plot of neuronal and glial gene scores in Patch-seq samples that passed cDNA QC, grouped by whether action potentials are detected in recording experiment, samples that failed QC, and negative controls. Gene scores are generated by aggregating the expression of top 50 neuronal marker genes or non-neuronal marker genes idenfied in human sensory neuron (42). (E) Pairwise correlation of Patch-seq data and published human DRG data. Bottom left panels show the normalized counts (log_2CPM) of individual genes in two datasets, each averaged across all cells/nuclei in the indicated cell population from the dataset. Top right panels show the Pearson's correlation coeffcient based on the average expression of genes between dataset pairs.

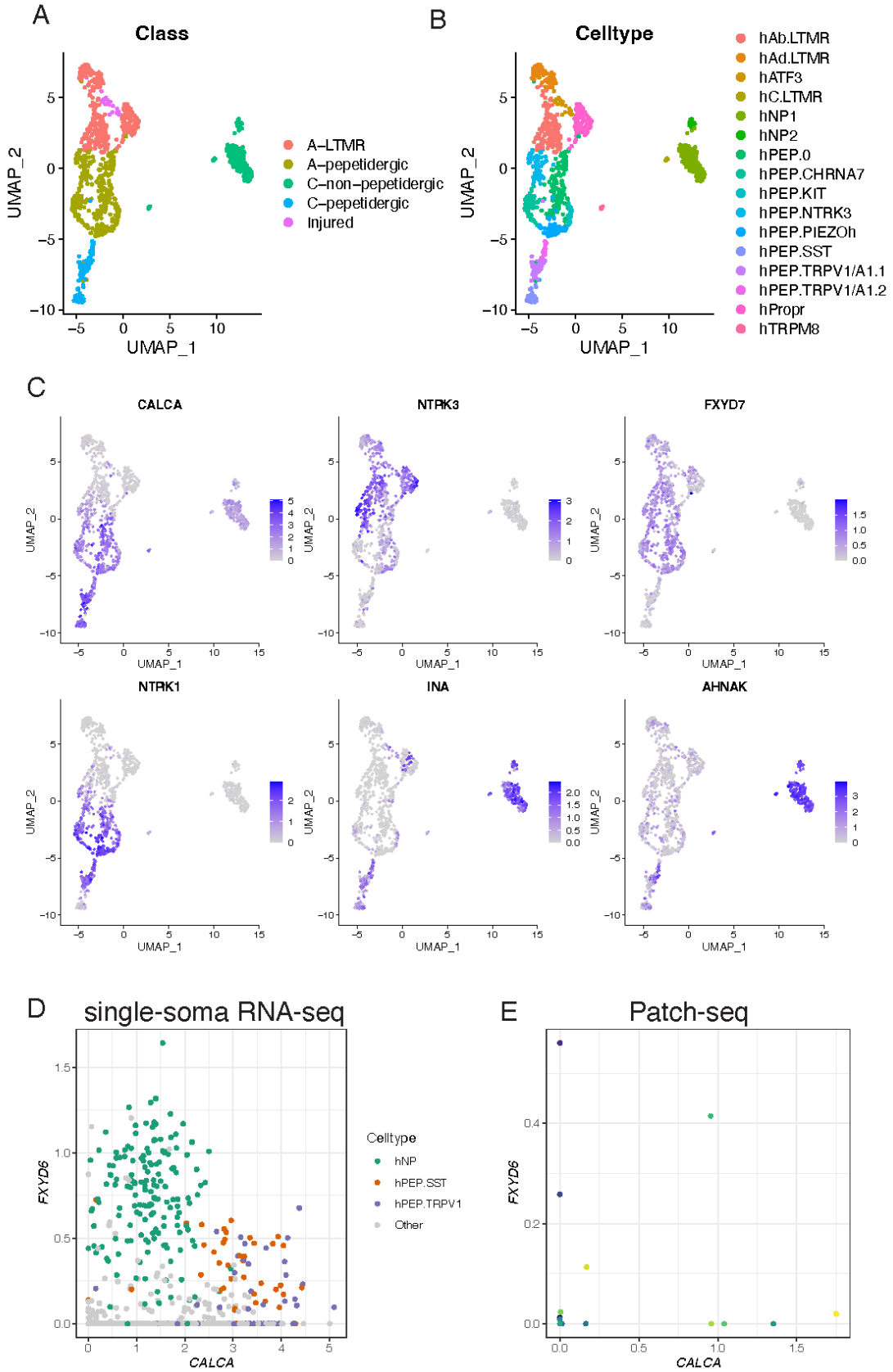
A
Class
UMAP_2
UMAP_1
A–LTMR
A–pepetidergic
C–non–pepetidergic
C–pepetidergic
Injured
B
Celltype
hAb.LTMR
hAd.LTMR
hATF3
hC.LTMR
hNP1
hNP2
hPEP.0
hPEP.CHRNA7
hPEP.KIT
hPEP.NTRK3
hPEP.PIEZOh
hPEP.SST
hPEP.TRPV1/A1.1
hPEP.TRPV1/A1.2
hPropr
hTRPM8
C
CALCA
NTRK3
FXYD7
NTRK1
INA
AHNAK
D
single-soma RNA-seq
FXYD6
CALCA
Celltype
hNP
hPEP.SST
hPEP.TRPV1
Other
E
Patch-seq
FXYD6
CALCA

Supplementary figure 4. Human DRG cell class marker genes. (A) UMAP of single-soma RNA-seq data, colored by four major cell classes and the injured cell state. (B) UMAP of single-soma RNA-seq data, colored by transcriptional cell types. (C) normalized counts (log_2CPM) of select cell class marker genes in single-soma RNA-seq data. (D) Scatter plot showing the normalized counts (log_2CPM) of *CALCA* and *FXYD6* in individual cells in single-soma RNA-seq. Cells are colored by transcriptional cell types. Cells of hPEP cell types have high expression of *CALCA* and low expression of *FXYD6*, whereas cells of hNP cell type have low expression of *CALCA* and high ecpression of *FXYD6*. (E) Scatter plot showing the normalized counts (log_2CPM) of *CALCA* and *FXYD6* in individual Patch-seq samples from cluster three. Cells expression *CALCA* and *FXYD6* are largely non-overlapping populations.

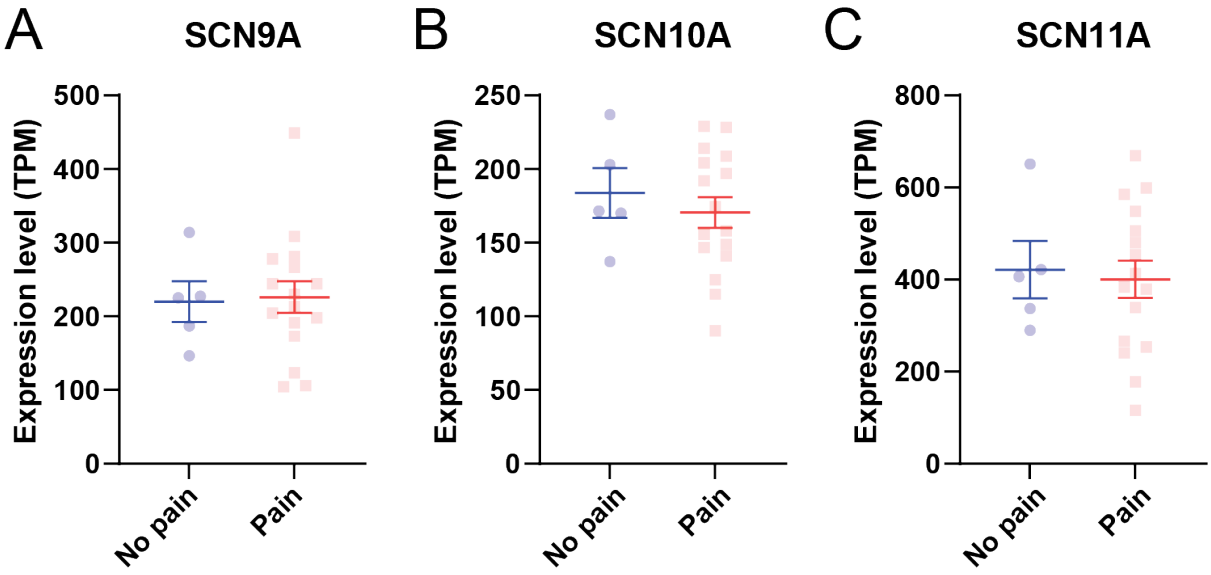

Supplementary Figure 5. Whole-tissue, bulk RNAseq of hDRG from cancer patients with and without pain shows no difference in *SCN9A*, *SCN10A*, and *SCN11A* expression. Whole tissue *SCN9A* (A), *SCN10A* (B), and *SCN11A* (C) expression in hDRG from cancer patients with or without neuropathic/reticular pain. Data re-analyzed from North et al., 2019 (30).

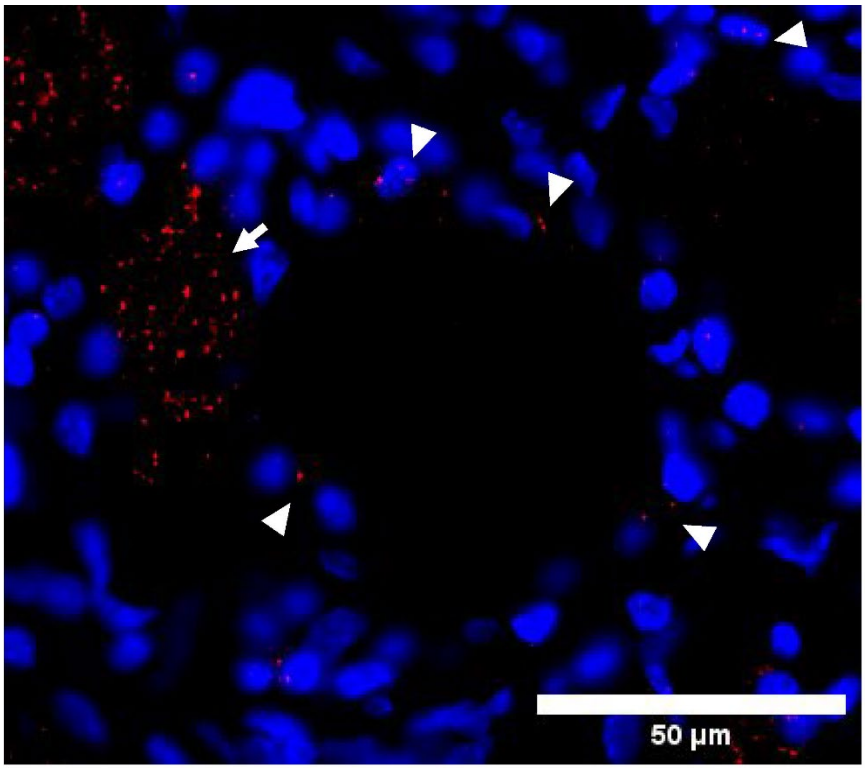

Supplementary Figure 6. SCN9A expression in satellite glial cells. Arrowheads point to mRNA probes detected in satellite glial cells that surround the hDRG neuronal cell bodies. Arrow point to an adjacent neuron that expresses *SCN9A*. Blue=DAPI, red=*SCN9A* transcripts.